JACS
JOURNAL OF THE AMERICAN CHEMICAL SOCIETY

ARTICLE

pubs.acs.org/JACS

Hydride-Shuttling Chain-Transfer Polymerization of Methacrylates Catalyzed by Metallocenium Enolate Metallacycle−Hydridoborate Ion Pairs

Yuetao Zhang,[†] Lucia Caporaso,[‡] Luigi Cavallo,*[,‡] and Eugene Y.-X. Chen*[,†]

[†]Department of Chemistry, Colorado State University, Fort Collins, Colorado 80523-1872, United States

[‡]Dipartimento di Chimica, Università di Salerno, Via Ponte don Melillo, I-84084 Fisciano (SA), Italy

ABSTRACT: Activation of 12 group IV metallocene bis(ester enolate) complexes with $B(C_6F_5)_3$ at room temperature (RT) affords quantitatively the corresponding isolable cationic eight-membered ester enolate metallacycles. This rapid two-step reaction consists of vinylogous hydride abstraction to form the anion $[HB(C_6F_5)_3]^-$, and nucleophilic addition of the second enolate ligand to the methacrylate resulted from loss of a hydride in the first enolate ligand to form the chelating cation. This activation methodology for generating the active species (structural models for resting intermediates involved in methacrylate polymerization) is rather general, as demonstrated by a broad substrate scope examined in this study, including group IV metallocene bis(ester enolate) complexes that varied metals (Ti, Zr, Hf), bridging atoms ($Ph_2C<$, $Ph_2Si<$, $Me_2C<$, $-CH_2CH_2-$), substituents (^{t}Bu, Et_3Si), substitution patterns (on 3-Cp and 2,7-Flu ring positions), and ligand symmetries (C_2, C_{2v}, C_1, and C_s), all of which lead to the clean formation of their corresponding cationic metallacycles. Comparative methyl methacrylate (MMA) polymerization studies have identified metallacycle **4**, $\{[Ph_2C(Cp)(2,7\text{-}^tBu_2\text{-}Flu)]Zr\text{-}[OC(O^iPr)=CMeCH_2C(Me_2)C(O^iPr)=O]\}^+[HB(C_6F_5)_3]^-$, as being the most active, efficient, and syndiospecific catalyst within the C_s-ligated catalysts. Kinetic experiments at room temperature show that the MMA polymerization by **4** follows first-order kinetics in both [MMA] and [Zr], consistent with a monometallic, intramolecular coordination−addition mechanism that involves the eight-membered ester enolate chelate resting state. Thermodynamic experiments at varied temperatures yield activation parameters of $\Delta H^{\ddagger} = 6.23$ kcal/mol, $\Delta S^{\ddagger} = -41.7$ eu, and $\Delta G^{\ddagger} = 17.6$ kcal/mol (273 K). As compared to *ansa*-Flu-Cp ligated chelating cations paired with more commonly used weakly coordinating anions such as $[MeB(C_6F_5)_3]^-$ and $[B(C_6F_5)_4]^-$, the same cations paired with the anion $[HB(C_6F_5)_3]^-$ behave differently in MMA polymerization in terms of activity, stereospecificity, and sensitivity to solvent polarity. Most uniquely, $[HB(C_6F_5)_3]^-$-based catalysts effect substantial internal chain-transfer reactions, especially for polymerizations carried out in toluene and in the presence of excess $B(C_6F_5)_3$, thus releasing polymer chains with a terminal double bond and achieving a catalytic polymerization. Computational results show the thermodynamics feasibility of the activation steps and the reversibility of the hydride abstraction step during activation, thus indicating that $[HB(C_6F_5)_3]^-$ can uniquely act as a weak hydride donor. The picture emerging from the combined experimental and theoretical study has led to a new hydride-shuttling chain-transfer mechanism promoted by the hydridoborate anion, involving a hydride addition and abstraction sequence through the borane center.

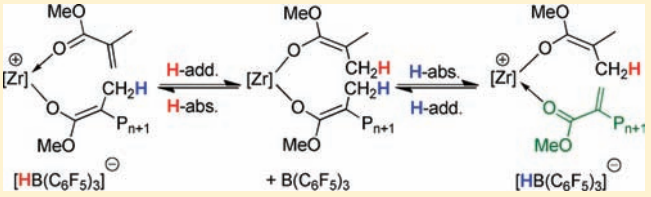

INTRODUCTION

Metal-catalyzed coordination polymerization of polar vinyl monomers[1,2] such as methyl methacrylate (MMA) is of current interest due to the ability (of coordination−addition polymerization) to rapidly produce high molecular weight (MW) polymers with controlled chain structures and stereomicrostructures.[1] Metallocene complexes, especially those of cationic group IV metallocene catalysts,[3] are the most active and stereoselective catalysts for this type of coordination polymerization.[1] However, an appropriate form of cationic catalysts, derived from activation of precatalysts with suitable activators, is critical for achieving a high degree of control over polymerization. Cationic alkyl or related catalysts,[4] typically derived from alkyl abstraction of dialkyl precatalysts by $B(C_6F_5)_3$ or $[Ph_3C][B(C_6F_5)_4]$, produce polar vinyl polymers, such as poly(methyl methacrylate) (PMMA), with uncontrolled MW and relatively broad MW distributions (MWDs).[1] On the other hand, cationic metallocene ester enolate complexes[5−8] are typically much more active [judged by turnover frequency, TOF (h^{-1}) = moles of substrate (monomer) converted to product (polymer) per mole of catalyst per hour], more efficient (judged by initiator efficiency, I^*), and more controlled (judged by the measured MW vs the calculated and by MWD) for polymerization of methacrylates[5−8] and (meth)acrylamides[9] than cationic alkyl complexes; this phenomenon has been attributed to the fact that such cationic ester enolate complexes bypass the slow initiation step involved in the polymerization by the alkyl complex (i.e., M−alkyl transfer to the coordinated monomer to form the cationic ester enolate species) and simulate the structure of true active propagating species.[10]

Received: October 30, 2010
Published: January 6, 2011

Chart 1. Twelve Cationic Ester Enolate Metallacycles Investigated in This Study

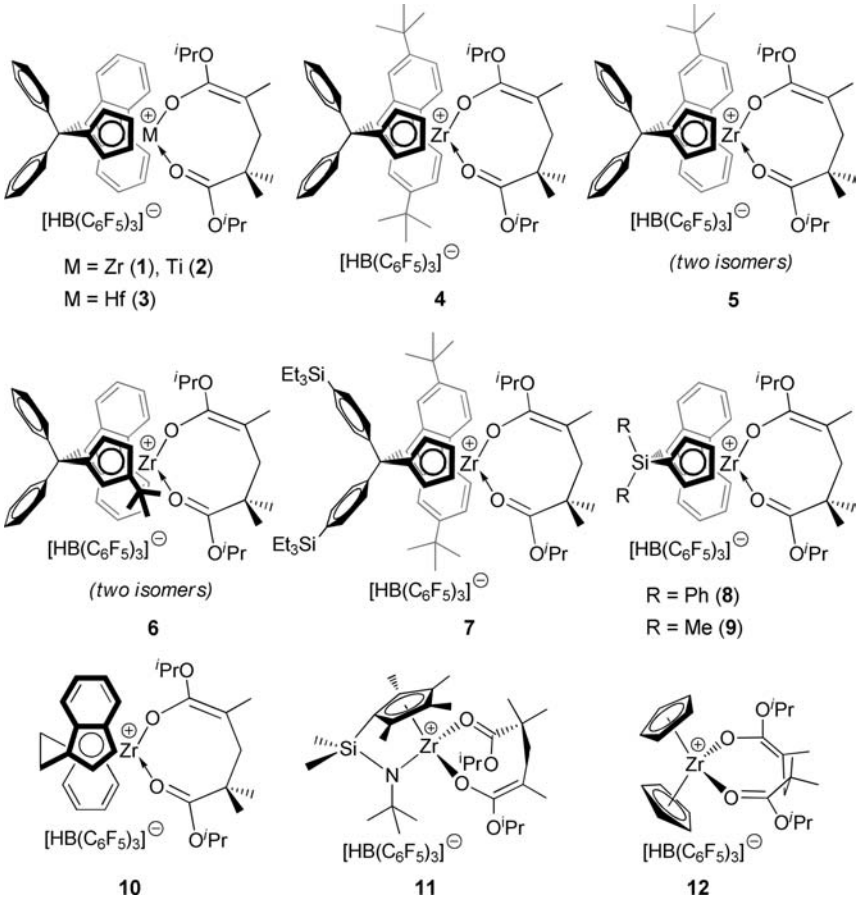

Several activation pathways have been established for generating cationic metallocene ester enolate catalysts from activation of the corresponding neutral complexes with appropriate activators. The first is alkyl abstraction of mono(ester enolate) metallocene alkyl complexes with strong Lewis acids such as $B(C_6F_5)_3$ and Cp_2ZrMe^+, in the presence of a donor (e.g., THF, which is typically required to stabilize the resulting ester enolate cation).[5−7,11] The second is activation of metallocene bis(ester enolate) precursors[12] with the strong Lewis acid $Al(C_6F_5)_3$ in the presence of monomer, which leads to the formation of dually active ion-pairs consisting of metallocene ester enolate cations and compatible enolaluminate anions enabling ion-pairing polymerization.[13] The third is protonolysis of metallocene bis(ester enolate) complexes with Brønsted acids such as $[HNMe_2Ph]^+[B(C_6F_5)_4]^-$ and $[H(Et_2O)_2]^+[B(C_6F_5)_4]^-$; this process generates the ester enolate cations stabilized by the coproduct ester and/or the base or donor solvent.[6a,b,14] The fourth is activation of metallocene bis(ester enolate) complexes by $[Ph_3C][B(C_6F_5)_4]$, which leads to a mixture of two cationic ester enolate species at low temperatures (one of which can be readily converted to the other upon warming or addition of monomer), as a result of simultaneous electrophilic addition of Ph_3C^+ to the enolate ligand and vinylogous hydride abstraction of the enolate ligand by Ph_3C^+.[14]

Much less is known about activation of metallocene bis(enolate) complexes with the strong Lewis acid $B(C_6F_5)_3$. Erker and co-workers reported that the reaction of unbridged, parent group IV metallocene bis(ketone enolate)s with $B(C_6F_5)_3$ forms direct adducts via electrophilic addition of the borane to the nucleophilic enolate carbon center.[15] We speculated that the reaction of metallocene bis(ester enolate)s with $B(C_6F_5)_3$ formed the same type of adducts,[12] based on elemental analysis and ^1H, ^{13}C, and ^{19}F NMR spectra data as the products were not crystallizable under various conditions. Clearly demonstrated direct-adduct formation between an ester enolate and an electrophile is known: for example, electrophilic addition of Ph_3C^+, via the *para*-carbon of Ph, to the nucleophilic enolate α-carbon of silicone ester enolates (i.e., silyl ketene acetals)[16] or that of zirconocene ester enolates (vide supra),[14] upon activation with $[Ph_3C][B(C_6F_5)_4]$ at low temperatures. Most recently, we noted that activation of an *ansa*-C_s-ligated zirconocene bis(ester enolate) with $B(C_6F_5)_3$ at room temperature conveniently produces the corresponding cationic eight-membered ester enolate chelate paired with the resulting anion $[HB(C_6F_5)_3]^-$, through the proposed vinylogous hydride abstraction of the enolate group by the borane.[14] However, neither the polymerization behavior of such species nor the scope of this activation methodology was investigated prior to this study. Motivated by both the attractive synthetic feature of this activation methodology (quantitative generation of the thermally stable, activated species in one-step at room temperature) and the importance of such an eight-membered chelate structure (which simulates the true active propagating species (resting state) in the methacrylate polymerization[1]), we set out in this study to investigate the scope of this activation by extending the metallocene bis(ester enolate) substrate to other group IV metallocene bis(ester enolate) precursors that varied metals (Ti, Zr, Hf), bridging atoms (Ph_2C<,

dx.doi.org/10.1021/ja109775v |*J. Am. Chem. Soc.* 2011, 133, 1572–1588

$Ph_2Si<$, $Me_2C<$, $-CH_2CH_2-$), substituents (^{t}Bu, Et_3Si), substitution patterns (on 3-Cp and 2,7-Flu ring positions), and ligand symmetries (C_2, C_{2v}, C_1, and C_s). This work resulted in successful isolation as well as spectroscopic and analytical characterization of 12 cationic metallocene eight-membered ester enolate metallacycles (Chart 1), which enabled our investigation of their MMA polymerization behavior and examination of the most active, efficient, and syndiospecific catalyst (complex **4**, Chart 1) in detail including kinetics and thermodynamics of polymerization. Theoretical/computational investigations added to our understanding of some unique features observed for the activation step, the behavior of the chelate cation paired with the anion $[HB(C_6F_5)_3]^-$, and the reversibility of the hydride abstraction step. Most excitingly, the synergistic experimental/computational approach we employed to the study of the $[HB(C_6F_5)_3]^-$-based catalyst system led to the discovery of a novel hydride-shuttling chain-transfer polymerization of methacrylates by group IV catalysts. Until now, promoting chain-transfer reactions for methacrylate polymerization (i.e., catalytic production of polymer chains) by group IV catalysts using various reagents (e.g., using enolizable organic acids) has been a challenge.[1,7,17]

EXPERIMENTAL SECTION

Materials, Reagents, and Methods. All syntheses and manipulations of air- and moisture-sensitive materials were carried out in flamed Schlenk-type glassware on a dual-manifold Schlenk line, on a high-vacuum line, or in an argon-filled glovebox. NMR-scale reactions (typically in a 0.02 mmol scale) were conducted in Teflon-valve-sealed J. Young-type NMR tubes. HPLC-grade organic solvents were first sparged extensively with nitrogen during filling 20 L solvent reservoirs and then dried by passage through activated alumina (for Et_2O, THF, and CH_2Cl_2) followed by passage through Q-5 supported copper catalyst (for toluene and hexanes) stainless steel columns. Benzene-d_6 and toluene-d_8 were dried over sodium/potassium alloy and vacuum-distilled or filtered, whereas CD_2Cl_2 and $CDCl_3$ were dried over activated Davison 4 Å molecular sieves. NMR spectra were recorded on Varian Inova 300 (FT 300 MHz, ^{1}H; 75 MHz, ^{13}C; 282 MHz, ^{19}F), 400 MHz, and 500 MHz spectrometers. Chemical shifts for ^{1}H and ^{13}C spectra were referenced to internal solvent resonances and are reported as parts per million relative to $SiMe_4$, whereas ^{19}F NMR spectra were referenced to external $CFCl_3$ and ^{11}B NMR spectra to $BF_3\cdot Et_2O$. Elemental analyses were performed by Desert Analytics, Tucson, AZ, and by Robertson Microlit Laboratories, Madison, NJ.

Methyl methacrylate (MMA), butylated hydroxytoluene (BHT-H, 2,6-di-*tert*-butyl-4-methylphenol), diisopropylamine, isopropyl isobutyrate, *n*-butyl lithium (1.6 M in hexanes), methyl magnesium bromide (3.0 M in diethyl ether), and other reagents were purchased from Aldrich Chemical Co and used as received unless otherwise specified as follows. MMA was degassed, dried over CaH_2 overnight, and vacuum-distillated; it was further purified by titration with neat tri(*n*-octyl)aluminum (Strem Chemical) to a yellow end point[18] and distillation under reduced pressure. The purified monomer was stored in a brown bottle inside a glovebox freezer at −30 °C. Diisopropylamine and isopropyl isobutyrate were dried over CaH_2, followed by vacuum distillation. BHT-H was recrystallized from hexanes prior to use. Tris(pentafluorophenyl)borane, $B(C_6F_5)_3$, trityl tetrakis(pentafluorophenyl)borate, $[Ph_3C][B(C_6F_5)_4]$, and diphenylmethylidene(cyclopentadienyl)(9-fluorenyl)zirconium dichloride, $[Ph_2C(Cp)(Flu)]ZrCl_2$, were obtained as research gifts from Boulder Scientific Co.; $B(C_6F_5)_3$ was further purified by recrystallization from hexanes at −30 °C, whereas the other two reagents were used as received. The adduct $THF\cdot B(C_6F_5)_3$ was prepared by addition of THF to a toluene solution of the borane at ambient temperature, followed by removal of the volatiles and drying in vacuo. Tris(pentafluorophenyl)alane, $Al(C_6F_5)_3$, as a 0.5 toluene adduct $Al(C_6F_5)_3\cdot(C_7H_8)_{0.5}$ (for vacuum-dried samples), was prepared by the reaction of $B(C_6F_5)_3$ and $AlMe_3$ in a 1:3 toluene/hexanes solvent mixture in quantitative yield;[19] this is the modified synthesis based on literature procedures.[20] Although we have experienced no incidents when handling this material, extra caution should be exercised, especially when dealing with the unsolvated form, because of its thermal and shock sensitivity.

Literature procedures were employed and modified for the preparation or generation of the following complexes: $Me_2C{=}C(O^iPr)OLi$,[12a,21] $[H(Et_2O)_2][B(C_6F_5)_4]$,[22] 2,7-di-*tert*-butylfluorene,[23] 2-*tert*-butylfluorene,[23] $[Ph_2C(Cp)(2,7\text{-}^tBu_2{-}Flu)]ZrCl_2$,[24] $[Ph_2C(Cp)(2\text{-}^tBu{-}Flu)]ZrCl_2$,[24] $[(p\text{-}Et_3SiC_6H_4)_2C(Cp)(2,7\text{-}^tBu_2{-}Flu)]ZrCl_2$,[25] $[Ph_2C(2\text{-}^tBu{-}Cp)(Flu)]ZrCl_2$,[26] $[Ph_2Si(Cp)(Flu)]ZrCl_2$,[27] $[Me_2Si(Cp)(Flu)]ZrCl_2$,[27] $[Ph_2C(Cp)(Flu)]HfCl_2$,[28] $[Ph_2C(Cp)(Flu)]ZrMe[OC(O^iPr){=}CMe_2]$,[5a] $[Ph_2C(Cp)(Flu)]M[OC(O^iPr){=}CMe_2]_2$ (M = Ti,[14] Zr,[5a] Hf[14]), $[Ph_2C(Cp)(2,7\text{-}^tBu_2{-}Flu)]Zr[OC(O^iPr){=}CMe_2]_2$,[14] $[Ph_2C(Cp)(2\text{-}^tBu{-}Flu)]Zr[OC(O^iPr){=}CMe_2]_2$,[14] $[Ph_2C(3\text{-}tert\text{-}Butyl\text{-}Cp)(Flu)]Zr[OC(O^iPr){=}CMe_2]_2$,[14] $[(p\text{-}Et_3SiPh)_2C(Cp)(2,7\text{-}^tBu_2{-}Flu)Zr[OC(O^iPr){=}CMe_2]_2$,[14] $[Ph_2Si(Cp)(Flu)]Zr[OC(O^iPr){=}CMe_2]_2$,[14] $[Me_2Si(Cp)(Flu)]Zr[OC(O^iPr){=}CMe_2]_2$,[14] *rac*-(EBI)$Zr[OC(O^iPr){=}CMe_2]_2$,[5e] (CGC)$Zr[OC(O^iPr){=}CMe_2]_2$,[12a] and $Cp_2Zr[OC(O^iPr){=}CMe_2]_2$ (Cp = η^5-cyclopentadienyl).[12b]

*$\{Ph_2C(Cp)(Flu)Zr[OC(O^iPr){=}CMeCH_2C(Me_2)C(O^iPr){=}O]\}^+[HB(C_6F_5)_3]^-$ (**1**).* For in situ generation of cationic complex **1**, a Teflon-valve-sealed J. Young-type NMR tube was charged with $Ph_2C(Cp)(Flu)Zr[OC(O^iPr){=}CMe_2]_2$ (14.9 mg, 0.02 mmol) and 0.3 mL of CD_2Cl_2. A 0.3 mL CD_2Cl_2 solution of $B(C_6F_5)_3$ (10.2 mg, 0.02 mmol) was added to this tube via pipet at ambient temperature to give instantaneously a black red solution; subsequent analysis of this solution by NMR showed the clean and quantitative formation of the eight-membered-ring chelate **1**. For isolation of the chelate **1**, a 20 mL glass vial was charged with the neutral bis(ester enolate) complex (0.16 mmol) and 4 mL of hexanes, while another vial was charged with $B(C_6F_5)_3$ (0.16 mmol) and 4 mL of toluene. The two vials were mixed via pipet at ambient temperature to give instantaneously a yellow solution and a red oil at the bottom of the vial. The top clear solution was decanted, and the red oil was washed by hexanes (3 × 5 mL). The hexanes were decanted, and complex **1** was obtained as a dark red solid in quantitative yield after drying under vacuum. Anal. Calcd for $C_{63}H_{48}BO_4F_{15}Zr$: C, 60.24; H, 3.85. Found: C, 59.98; H, 4.06.

*^{1}H NMR (CD_2Cl_2, 23 °C) for **1**.* δ 8.39 (d, J = 8.4 Hz, 1H, Flu), 8.27 (d, J = 8.4 Hz, 1H, Flu), 7.99 (d, J = 7.6 Hz, 1H, Ph), 7.93 (d, J = 8.0 Hz, 3H, Ph), 7.60−7.18 (m, 10H, Flu, Ph), 6.63 (d, J = 8.4 Hz, 1H, Flu), 6.62 (d, J = 8.8 Hz, 1H, Flu), 6.50 (m, 1H, Cp), 5.99 (m, 1H, Cp), 5.89 (m, 2H, Cp), 4.10 (sept, J = 6.2 Hz, 1H, C*H*Me$_2$), 3.63 (q, J = 90.6 Hz, 1H, B*H*), 3.23 (sept, J = 6.2 Hz, 1H, C*H*Me$_2$), 2.25 (d, ^2J = 14.8 Hz, 1H, CH_2), 1.54 (d, ^2J = 15.2 Hz, 1H, CH_2), 1.43 (s, 3H, =C*Me*), 1.28 (s, 3H, C*Me*$_2$), 1.19 (d, J = 6.0 Hz, 3H, CH*Me*$_2$), 1.16 (s, 3H, C*Me*$_2$), 1.15 (d, J = 6.8 Hz, 3H, CH*Me*$_2$), 1.06 (d, J = 6.4 Hz, 3H, CH*Me*$_2$), 0.78 (d, J = 6.0 Hz, 3H, CH*Me*$_2$). ^{1}H NMR (C_7D_8, 23 °C): δ 7.93 (d, J = 8.1 Hz, 1H, Flu), 7.87 (d, J = 8.4 Hz, 1H, Flu), 7.71 (d, J = 7.8 Hz, 1H, Ph), 7.64 (d, J = 7.5 Hz, 1H, Ph), 7.47 (t, J = 8.5 Hz, 2H, Flu), 7.22−6.87 (m, 12H, Ph, Flu), 6.33 (q, J = 2.9 Hz, 1H, Cp), 5.81 (q, J = 2.7 Hz, 1H, Cp), 5.74 (q, J = 2.7 Hz, 1H, Cp), 5.57 (q, J = 2.9 Hz, 1H, Cp), 4.40 (s, br, 1H, B*H*), 3.83 (sept, J = 6.2 Hz, 1H, C*H*Me$_2$), 3.10 (sept, J = 6.2 Hz, 1H, C*H*Me$_2$), 2.06 (d, J = 15.3 Hz, 1H, CH_2), 1.44 (s, 3H, =C*Me*), 1.25 (d, J = 15.3 Hz, 1H, CH_2), 0.99 (s, 3H, C*Me*$_2$), 0.98 (d, J = 6.3 Hz, 3H, CH*Me*$_2$), 0.88 (s, 3H, C*Me*$_2$), 0.86 (d, J = 6.3 Hz, 3H, CH*Me*$_2$), 0.76 (d, J = 6.0 Hz, 3H, CH*Me*$_2$), 0.69 (d, J = 6.0 Hz, 3H, CH*Me*$_2$). ^{19}F NMR (CD_2Cl_2, 23 °C): δ −132.1 (d, J_{F-F} = 22.3 Hz, 6F, *o*-F), −162.9 (t, J_{F-F} = 20.3 Hz, 3F, *p*-F), −165.8 (m, 6F, *m*-F). ^{19}F NMR (C_7D_8, 23 °C): δ −132.5 (d, $^3J_{F-F}$ = 21.7 Hz, 6F, *o*-F), −164.3 (t, $^3J_{F-F}$ = 20.4 Hz, 3F, *p*-F), −167.0 (m, 6F, *m*-F). ^{13}C NMR (CD_2Cl_2, 23 °C): δ 191.2 [*C*(O^{i}Pr)=O], 155.6 [OC(O^{i}Pr)=], 144.5, 130.2, 130.1, 130.0, 129.58, 129.55, 129.3, 128.4, 127.4, 127.11, 127.05, 125.2, 125.1, 124.9, 124.4, 124.2, 123.7, 123.5, 123.4, 122.2, 117.7, 117.6, 114.2, 107,4, 103.9, 81.16 (a total of 26 resonances observed for the Flu, Ph, C_6F_5, and Cp carbons; broad resonances for the

C_6F_5 groups due to C−F coupling omitted), 86.09 (=*C*Me), 76.64, 68.93 (*C*HMe$_2$), 60.10 (*C*Ph$_2$), 46.33 (*C*Me$_2$), 40.76 (*C*H$_2$), 31.89 (*C*Me$_2$), 24.79 (*C*Me$_2$), 22.55, 21.91, 21.38, 21.35 (CH*Me*$_2$), 17.38 (=C*Me*). ^{11}B NMR (CD_2Cl_2, 23 °C): δ −25.6 (d, $^1J_{B-H}$ = 89.8 Hz).

*{Ph$_2$C(Cp)(Flu)Ti[OC(O^{i}Pr)=CMeCH$_2$C(Me$_2$)C(O^{i}Pr)=O]}$^+$[HB(C$_6$F$_5$)$_3$]$^-$ (**2**).* In situ generation and isolation of the dark red titanium complex **2** were carried out in the same manner as described for the zirconium complex **1**. Anal. Calcd for $C_{63}H_{48}BO_4F_{15}Ti$: C, 62.40; H, 3.99. Found: C, 62.63; H, 4.21.

*^{1}H NMR (CD_2Cl_2, 23 °C) for **2**.* δ 8.34 (d, J = 8.0 Hz, 1H, Flu), 8.13 (d, J = 8.0 Hz, 1H, Flu), 8.07 (d, J = 8.0 Hz, 1H, Ph), 7.99 (d, J = 8.0 Hz, 1H, Ph), 7.93 (d, J = 7.6 Hz, 2H, Ph), 7.66−7.36 (m, 8H, Flu, Ph), 7.11 (t, J = 8.0 Hz, 1H, Flu), 7.05 (t, J = 8.0 Hz, 1H, Flu), 6.71 (q, J = 3.1 Hz, 1H, Cp), 6.44 (d, J = 8.8 Hz, 1H, Flu), 6.36 (d, J = 8.8 Hz, 1H, Flu), 5.73 (q, J = 2.5 Hz, 1H, Cp), 5.69 (q, J = 2.9 Hz, 1H, Cp), 5.60 (q, J = 2.7 Hz, 1H, Cp), 3.77 (sept, J = 6.2 Hz, 1H, C*H*Me$_2$), 3.62 (q, J = 89.9 Hz, 1H, B*H*), 3.01 (sept, J = 6.2 Hz, 1H, C*H*Me$_2$), 2.66 (d, ^2J = 14.8 Hz, 1H, C*H*$_2$), 1.46 (d, ^2J = 14.4 Hz, 1H, C*H*$_2$), 1.45 (s, 3H, =C*Me*), 1.33 (s, 3H, C*Me*$_2$), 1.13 (s, 3H, C*Me*$_2$), 1.10 (d, J = 6.0 Hz, 6H, CH*Me*$_2$), 1.07 (d, J = 6.4 Hz, 3H, CH*Me*$_2$), 0.74 (d, J = 6.4 Hz, 3H, CH*Me*$_2$). ^{19}F NMR (CD_2Cl_2, 23 °C): δ −132.2 (d, J_{F-F}=20.7 Hz, 6F, *o*-F), −163.0 (t, J_{F-F}=20.3 Hz, 3F, *p*-F), −165.8 (m, 6F, *m*-F). ^{13}C NMR (CD_2Cl_2, 23 °C): δ 190.3 [*C*(O^{i}Pr)=O], 161.7 [OC(O^{i}Pr)=], 144.0, 143.7, 134.0, 133.8, 130.6, 130.2, 130.1, 129.9, 129.8, 129.4, 129.3, 128.9, 128.6, 128.5, 127.4, 127.34, 127.31, 127.1, 124.8, 123.8, 123.6, 122.4, 120.3, 118.3, 113.6, 107.8, 105.0, 84.13 (a total of 28 resonances observed for the Flu, Ph, C_6F_5, and Cp carbons; broad resonances for the C_6F_5 groups due to C−F coupling omitted), 86.08 (=*C*Me), 74.00, 69.37 (*C*HMe$_2$), 59.73 (*C*Ph$_2$), 44.88 (*C*Me$_2$), 40.16 (*C*H$_2$), 32.34 (*C*Me$_2$), 25.22 (*C*Me$_2$), 22.52, 22.33, 21.55, 21.12 (CH*Me*$_2$), 17.49 (=C*Me*). ^{11}B NMR (CD_2Cl_2, 23 °C): δ −25.6 (d, $^1J_{B-H}$ = 89.8 Hz).

*{Ph$_2$C(Cp)(Flu)Hf[OC(O^{i}Pr)=CMeCH$_2$C(Me$_2$)C(O^{i}Pr)=O]}$^+$[HB(C$_6$F$_5$)$_3$]$^-$ (**3**).* In situ generation and isolation of the dark red hafnium complex **3** were carried out in the same manner as described for the zirconium complex **1**. Anal. Calcd for $C_{63}H_{48}BO_4F_{15}Hf$: C, 56.33; H, 3.60. Found: C, 56.17; H, 3.87.

*^{1}H NMR (CD_2Cl_2, 23 °C) for **3**.* δ 8.35 (d, J = 8.4 Hz, 1H, Flu), 8.24 (d, J = 8.4 Hz, 1H, Flu), 7.98 (d, J = 7.2 Hz, 1H, Ph), 7.94 (d, J = 7.2 Hz, 3H, Ph), 7.59−7.16 (m, 10H, Flu, Ph), 6.69 (d, J = 8.4 Hz, 1H, Flu), 6.68 (d, J = 8.8 Hz, 1H, Flu), 6.52 (q, J = 3.1 Hz, 1H, Cp), 5.92 (q, J = 2.9 Hz, 1H, Cp), 5.86−5.82 (m, 2H, Cp), 4.12 (sept, J = 6.3 Hz, 1H, C*H*Me$_2$), 3.62 (q, J = 91.4 Hz, 1H, B*H*), 3.26 (sept, J = 6.2 Hz, 1H, C*H*Me$_2$), 2.24 (d, ^2J = 15.2 Hz, 1H, C*H*$_2$), 1.56 (d, ^2J = 15.2 Hz, 1H, C*H*$_2$), 1.45 (s, 3H, =C*Me*), 1.30 (s, 3H, C*Me*$_2$), 1.21 (d, J = 6.4 Hz, 3H, CH*Me*$_2$), 1.19 (d, J = 6.4 Hz, 3H, CH*Me*$_2$), 1.15 (s, 3H, C*Me*$_2$), 1.07 (d, J = 6.4 Hz, 3H, CH*Me*$_2$), 0.80 (d, J = 6.0 Hz, 3H, CH*Me*$_2$). ^{19}F NMR (CD_2Cl_2, 23 °C): δ −132.2 (d, J_{F-F} = 21.2 Hz, 6F, *o*-F), −163.0 (t, J_{F-F} = 20.3 Hz, 3F, *p*-F), −165.9 (m, 6F, *m*-F). ^{13}C NMR (CD_2Cl_2, 23 °C): δ 192.1 [*C*(O^{i}Pr)=O], 154.9 [OC(O^{i}Pr)=], 144.7, 144.7, 130.2, 130.08, 130.05, 130.0, 129.5, 129.3, 129.2, 128.39, 128.38, 127.09, 127.06, 126.99, 124.9, 124.8, 123.9, 123.6, 122.7, 122.2, 121.6, 121.0, 117.0, 116.8, 116.0, 104.7, 101.4, 80.81 (a total of 28 resonances observed for the Flu, Ph, C_6F_5, and Cp carbons; broad resonances for the C_6F_5 groups due to C−F coupling omitted), 86.24 (=*C*Me), 77.47, 68.99 (*C*HMe$_2$), 60.13 (*C*Ph$_2$), 46.67 (*C*Me$_2$), 40.26 (*C*H$_2$), 31.84 (*C*Me$_2$), 24.97 (*C*Me$_2$), 22.57, 22.08, 21.43, 21.38 (CH*Me*$_2$), 17.30 (=C*Me*). ^{11}B NMR (CD_2Cl_2, 23 °C): δ −25.6 (d, $^1J_{B-H}$ = 89.8 Hz).

*{[Ph$_2$C(Cp)(2,7-^{t}Bu$_2$−Flu)]Zr[OC(O^{i}Pr)=CMeCH$_2$C(Me$_2$)C(O^{i}Pr)=O]}$^+$[HB(C$_6$F$_5$)$_3$]$^-$ (**4**).* This species was previously generated by in situ NMR-scale reaction but was neither isolated nor analytically characterized.[14] For isolation of chelate **4**, the same procedures as the isolation of complex **1** described above were used to produce **4** as a dark red solid in quantitative yield. Anal. Calcd for $C_{71}H_{64}BO_4F_{15}Zr$: C, 62.32; H, 4.71. Found: C, 62.60; H, 5.01.

*^{1}H NMR (CD_2Cl_2, 23 °C) for **4**.* δ 8.26 (d, J = 8.8 Hz, 1H, Flu), 8.09 (d, J = 8.8 Hz, 1H, Flu), 8.02 (d, J = 8.0 Hz, 1H, Ph), 7.98 (d, J = 8.0 Hz, 1H, Ph), 7.93 (d, J = 7.6 Hz, 2H, Ph), 7.62−7.39 (m, 8H, Flu, Ph), 6.62 (s, 1H, Flu), 6.54 (s, 1H, Flu), 6.54−6.52 (m, 1H, Cp), 5.97 (q, J = 2.9 Hz, 1H, Cp), 5.92 (q, J = 2.8 Hz, 1H, Cp), 5.84 (q, J = 2.8 Hz, 1H, Cp), 4.26 (sept, J = 6.0 Hz, 1H, C*H*Me$_2$), 3.60 (q, J = 91.6 Hz, 1H, B*H*), 3.31 (sept, J = 6.2 Hz, 1H, C*H*Me$_2$), 2.44 (d, ^2J = 15.2 Hz, 1H, C*H*$_2$), 1.58 (d, ^2J = 14.8 Hz, 1H, C*H*$_2$), 1.44 (s, 3H, =C*Me*), 1.30 (s, 3H, C*Me*$_2$), 1.24 (d, J = 6.4 Hz, 3H, CH*Me*$_2$), 1.18 (s, 3H, C*Me*$_2$), 1.10 (d, J = 6.4 Hz, 3H, CH*Me*$_2$), 1.07 (s, 18H, ^{t}Bu), 1.04 (d, J = 6.4 Hz, 3H, CH*Me*$_2$), 0.84 (d, J = 6.0 Hz, 3H, CH*Me*$_2$). ^{19}F NMR (CD_2Cl_2, 23 °C): δ −132.2 (d, J_{F-F} = 22.3 Hz, 6F, *o*-F), −163.1 (t, J_{F-F} = 20.3 Hz, 3F, *p*-F), −165.9 (m, 6F, *m*-F). ^{13}C NMR (CD_2Cl_2, 23 °C): δ 190.7 [*C*(O^{i}Pr)=O], 155.8 [OC(O^{i}Pr)=], 153.5, 153.2, 144.0, 143.9, 129.7, 129.64, 129.59, 129.4, 128.0, 126.8, 126.7, 125.6, 124.2, 124.0, 123.7, 122.7, 121.8, 121.4, 120.7, 119.0, 117.6, 117.2, 115.2, 106.0, 102.8, 82.24 (Flu, Ph, C_6F_5, and Cp carbons; broad resonances for the C_6F_5 groups due to C−F coupling omitted), 86.52 (=*C*Me), 75.51, 68.87 (*C*HMe$_2$), 59.25 (*C*Ph$_2$), 47.59 (*C*Me$_2$), 40.58 (*C*H$_2$), 35.59, 35.43 (*C*(CH$_3$)$_3$), 31.93 (*C*Me$_2$), 30.82, 30.75 (C(*C*H$_3$)$_3$), 24.76 (*C*Me$_2$), 22.46, 22.10, 21.82, 21.33 (CH*Me*$_2$), 16.92 (=C*Me*). ^{11}B NMR (CD_2Cl_2, 23 °C): δ −25.4 (d, $^1J_{B-H}$ = 93.7 Hz).

*{[Ph$_2$C(Cp)(2-^{t}Bu−Flu)]Zr[OC(O^{i}Pr)=CMeCH$_2$C(Me$_2$)C(O^{i}Pr)=O]}$^+$[HB(C$_6$F$_5$)$_3$]$^-$ (**5**).* In situ generation and isolation of dark red chelate **5**, as two isomers A and B in a 4:5 ratio, were carried out in the same manner as described for complex **1**. Anal. Calcd for $C_{67}H_{56}BO_4F_{15}Zr$: C, 61.33; H, 4.30. Found: C, 61.05; H, 4.47.

*^{1}H NMR (CD_2Cl_2, 23 °C) for **5**.* δ 8.35, 8.22 (d, J = 8.4 Hz, 1H, Flu), 8.29, 8.16 (d, J = 8.8 Hz, 1H, Flu), 8.04−7.91 (m, 4H, Ph), 7.68−7.13 (m, 9H, Flu, Ph), 6.67, 6.65 (d, J = 8.4 Hz, 1H, Flu), 6.60, 6.54 (s, 1H, Flu), 6.61, 6.47 (m, 1H, Cp), 5.98−5.95 (m, 1H, Cp), 5.91 (m, 1H, Cp), 5.86, 5.84 (m, 1H, Cp), 4.22, 4.11 (sept, J = 6.2 Hz, 1H, C*H*Me$_2$), 3.63 (q, J = 90.2 Hz, 1H, B*H*), 3.28, 3.27 (sept, J = 6.2 Hz, 1H, C*H*Me$_2$), 2.38, 2.31 (d, ^2J = 14.8 Hz, 1H, C*H*$_2$), 1.58, 1.55 (d, ^2J = 14.8 Hz, 1H, C*H*$_2$), 1.45, 1.43 (s, 3H, =C*Me*), 1.31, 1.28 (s, 3H, C*Me*$_2$), 1.23 (d, J = 6.0 Hz, 3H, CH*Me*$_2$), 1.19 (d, J = 6.0 Hz, 3H, CH*Me*$_2$), 1.18, 1.17 (s, 3H, C*Me*$_2$), 1.09−1.05 (m, 6H, CH*Me*$_2$), 1.08 (s, 9H, ^{t}Bu), 0.81, 0.80 (d, J = 6.0 Hz, 3H, CH*Me*$_2$). ^{19}F NMR (CD_2Cl_2, 23 °C): δ −132.1 (d, J_{F-F} = 20.9 Hz, 6F, *o*-F), −163.0 (t, J_{F-F} = 20.3 Hz, 3F, *p*-F), −165.8 (m, 6F, *m*-F). ^{13}C NMR (CD_2Cl_2, 23 °C): δ 191.4, 190.8 [*C*(O^{i}Pr)=O], 156.4, 155.4 [OC(O^{i}Pr)=], 154.5, 154.2, 144.6, 144.4, 130.1, 129.9, 129.7, 129.6, 129.3, 129.2, 128.4, 127.40, 127.35, 126.9, 126.8, 126.0, 125.3, 125.2, 124.8, 124.6, 124.5, 124.32, 124.26, 124.1, 123.8, 123.6, 123.4, 123.0, 122.4, 122.2, 120.6, 119.6, 118.3, 118.1, 117.4, 117.2, 115.3, 114.5, 107.4, 106.7, 103.8, 103.2, 82.19, 81.37 (a total of 44 resonances observed for the Flu, Ph, C_6F_5, and Cp carbons; broad resonances for the C_6F_5 groups due to C−F coupling omitted), 87.51, 85.62 (=*C*Me), 76.40, 76.17, 69.10, 68.99 (*C*HMe$_2$), 60.03, 59.85 (*C*Ph$_2$), 48.14, 46.10 (*C*Me$_2$), 41.00, 40.71 (*C*H$_2$), 36.01, 35.92 (*C*(CH$_3$)$_3$), 32.22, 31.84 (*C*Me$_2$), 31.23, 31.14 (C(*C*H$_3$)$_3$), 25.17, 24.88 (*C*Me$_2$), 22.62, 22.53, 22.16, 22.06, 21.47, 21.36 (CH*Me*$_2$), 17.61, 17.05 (=C*Me*). ^{11}B NMR (CD_2Cl_2, 23 °C): δ −25.5 (d, $^1J_{B-H}$ = 88.0 Hz).

*Ph$_2$C(3-tert-Butyl−Cp)(Flu)Zr$^+$[OC(O^{i}Pr)=CMeCH$_2$C(Me$_2$)C(O^{i}Pr)=O][HB(C$_6$F$_5$)$_3$]$^-$ (**6**).* In situ generation and isolation of dark red chelate **6**, as two isomers A and B in a 2:3 ratio, were carried out in the same manner as described for complex **1**. Anal. Calcd for $C_{67}H_{56}BO_4F_{15}Zr$: C, 61.33; H, 4.30. Found: C, 61.07; H, 4.04.

*^{1}H NMR (CD_2Cl_2, 23 °C) for **6** (Only Key Resonances Shown).* Isomer A, δ 8.32 (d, J = 8.4 Hz, 1H, Flu), 6.41 (m, 1H, Cp), 5.99 (m, 1H, Cp), 5.78 (m, 1H, Cp), 4.20 (sept, J = 6.2 Hz, 1H, C*H*Me$_2$), 3.62 (q, J = 88.4 Hz, 1H, B*H*), 3.29 (sept, J = 6.2 Hz, 1H, C*H*Me$_2$), 2.33 (d, ^2J = 15.2 Hz, 1H, C*H*$_2$), 1.67 (d, ^2J = 15.2 Hz, 1H, C*H*$_2$), 1.01 (s, 9H, ^{t}Bu); isomer B, δ 8.28 (d, J = 8.4 Hz, 1H, Flu), 5.99 (m, 1H, Cp), 5.90 (m, 1H, Cp), 5.82 (m, 1H, Cp), 4.09 (sept, J = 6.2 Hz, 1H, C*H*Me$_2$), 3.62 (q, J = 88.4 Hz, 1H, B*H*), 3.16 (sept, J = 6.2 Hz, 1H, C*H*Me$_2$), 2.42 (d, ^2J = 15.2 Hz, 1H, C*H*$_2$), 1.68 (d, ^2J = 15.2 Hz, 1H, C*H*$_2$), 1.10 (s, 9H, ^{t}Bu). ^{19}F NMR (CD_2Cl_2, 23 °C): δ −132.2 (d, J_{F-F} = 22.6 Hz, 6F, *o*-F), −163.0 (t, J_{F-F} = 19.6 Hz, 3F, *p*-F), −165.9 (m, 6F, *m*-F). ^{13}C NMR (CD_2Cl_2, 23 °C), isomer A,

δ 191.1 [C(O^{i}Pr)═O], 155.6 [OC(O^{i}Pr)═], 85.16 (═CMe), 76.04, 69.20 (CHMe$_2$), 59.06 (CPh$_2$), 45.93 (CMe$_2$), 40.41 (CH$_2$), 33.24 (C(CH$_3$)$_3$), 32.16 (CMe$_2$), 31.46 (C(CH$_3$)$_3$), 23.44 (CMe$_2$), 22.47, 22.34, 21.85, 21.42 (CHMe$_2$), 17.02 (═CMe); isomer B, δ 191.3 [C(O^{i}Pr)═O], 157.3 [OC(O^{i}Pr)═], 89.73 (═CMe), 77.18, 70.51 (CHMe$_2$), 59.42 (CPh$_2$), 46.65 (CMe$_2$), 38.94 (CH$_2$), 33.41 (C(CH$_3$)$_3$), 31.12 (CMe$_2$), 30.48 (C(CH$_3$)$_3$), 24.65 (CMe$_2$), 22.39, 22.09, 21.79, 21.14 (CHMe$_2$), 19.04 (═CMe). ^{11}B NMR (CD$_2$Cl$_2$, 23 °C): δ −25.6 (d, $^1J_{B-H}$ = 82.3 Hz).

{[(p-Et$_3$SiPh)$_2$C(Cp)(2,7-^{t}Bu$_2$−Flu)Zr[OC(O^{i}Pr)═CMeCH$_2$C(Me$_2$)-C(O^{i}Pr)═O]}$^+$[HB(C$_6$F$_5$)$_3$]$^-$ (**7**). In situ generation and isolation of dark red chelate **7** were carried out in the same manner as described for complex **1**. Anal. Calcd for $C_{83}H_{92}BO_4F_{15}Si_2Zr$: C, 62.43; H, 5.81. Found: C, 62.15; H, 5.93.

*^{1}H NMR (CD$_2$Cl$_2$, 23 °C) for **7**.* δ 8.26 (d, *J* = 8.8 Hz, 1H, Flu), 8.10 (d, *J* = 8.8 Hz, 1H, Flu), 8.01 (dd, ^3J = 7.6 Hz, ^4J = 1.6 Hz, 1H, Ph), 7.98 (dd, ^3J = 7.6 Hz, ^4J = 1.6 Hz, 1H, Ph), 7.93 (d, *J* = 8.0 Hz, 2H, Ph), 7.73 (d, *J* = 9.0 Hz, 1H, Flu), 7.71 (d, *J* = 9.0 Hz, 1H, Flu), 7.61 (d, *J* = 8.0 Hz, 2H, Ph), 7.60 (dd, ^3J = 8.4 Hz, ^4J = 1.2 Hz, 1H, Ph), 7.52 (dd, ^3J = 8.8 Hz, ^4J = 1.2 Hz, 1H, Ph), 6.60 (s, 1H, Flu), 6.52 (s, 1H, Flu), 6.53−6.51 (m, 1H, Cp), 5.98 (q, *J* = 2.9 Hz, 1H, Cp), 5.92 (q, *J* = 2.7 Hz, 1H, Cp), 5.84 (q, *J* = 2.6 Hz, 1H, Cp), 4.26 (sept, *J* = 6.2 Hz, 1H, CHMe$_2$), 3.60 (q, *J* = 90.1 Hz, 1H, BH), 3.32 (sept, *J* = 6.2 Hz, 1H, CHMe$_2$), 2.44 (d, ^2J = 15.2 Hz, 1H, CH$_2$), 1.58 (d, ^2J = 14.4 Hz, 1H, CH$_2$), 1.44 (s, 3H, ═CMe), 1.31 (s, 3H, CMe$_2$), 1.24 (d, *J* = 6.4 Hz, 3H, CHMe$_2$), 1.18 (s, 3H, CMe$_2$), 1.11 (d, *J* = 6.4 Hz, 3H, CHMe$_2$), 1.07 (s, 18H, ^{t}Bu), 1.04 (d, *J* = 6.4 Hz, 3H, CHMe$_2$), 1.025 (t, *J* = 8.0 Hz, 9H, SiCH$_2$CH$_3$), 1.017 (t, *J* = 8.0 Hz, 9H, SiCH$_2$CH$_3$), 0.88−0.81 (m, 15H, CHMe$_2$, SiCH$_2$CH$_3$). ^{19}F NMR (CD$_2$Cl$_2$, 23 °C): δ −132.2 (d, J_{F-F} = 21.2 Hz, 6F, *o*-F), −163.1 (t, J_{F-F} = 20.3 Hz, 3F, *p*-F), −165.9 (m, 6F, *m*-F). ^{13}C NMR (CD$_2$Cl$_2$, 23 °C): δ 190.7 [C(O^{i}Pr)═O], 155.8 [OC(O^{i}Pr)═], 153.4, 153.2, 144.3, 144.2, 138.1, 135.7, 135.6, 135.3, 129.0, 128.8, 126.1, 126.0, 125.4, 124.2, 124.0, 123.8, 122.6, 121.8, 121.4, 120.8, 119.1, 117.6, 117.2, 115.0, 106.0, 102.8, 82.14 (a total of 27 resonances observed for the Flu, Ph, C$_6$F$_5$, and Cp carbons; broad resonances for the C$_6$F$_5$ groups due to C−F coupling omitted), 86.46 (═CMe), 75.48, 68.81 (CHMe$_2$), 59.18 (CPh$_2$), 47.63 (CMe$_2$), 40.55 (CH$_2$), 35.59, 35.43 (C(CH$_3$)$_3$), 31.90 (CMe$_2$), 30.93, 30.88 (C(CH$_3$)$_3$), 24.74 (CMe$_2$), 22.44, 22.08, 21.80, 21.31 (CHMe$_2$), 16.92 (═CMe), 7.36 (SiCH$_2$CH$_3$), 3.45 (SiCH$_2$CH$_3$). ^{11}B NMR (CD$_2$Cl$_2$, 23 °C): δ −25.6 (d, $^1J_{B-H}$ = 89.8 Hz).

{[Ph$_2$Si(Cp)(Flu)]Zr[OC(O^{i}Pr)═CMeCH$_2$C(Me$_2$)C(O^{i}Pr)═O]}$^+$[HB-(C$_6$F$_5$)$_3$]$^-$ (**8**). In situ generation and isolation of orange chelate **8** were carried out in the same manner as described for complex **1**. Anal. Calcd for $C_{62}H_{48}BO_4F_{15}SiZr$: C, 58.54; H, 3.80. Found: C, 58.71; H, 3.88.

*^{1}H NMR (CD$_2$Cl$_2$, 23 °C) for **8**.* δ 8.31 (d, *J* = 8.4 Hz, 1H, Flu), 8.22−8.17 (m, 3H, Flu, Ph), 7.67−7.58 (m, 6H, Flu, Ph), 7.49 (t, *J* = 7.6 Hz, 2H, Ph), 7.31−7.20 (m, 4H, Flu, Ph), 7.08 (t, *J* = 8.6 2H, Flu), 6.92 (m, 1H, Cp), 6.07 (m, 1H, Cp), 6.04 (m, 1H, Cp), 5.95 (m, 1H, Cp), 4.09 (sept, *J* = 6.2 Hz, 1H, CHMe$_2$), 3.65 (s, br, 1H, BH), 3.24 (sept, *J* = 6.2 Hz, 1H, CHMe$_2$), 2.28 (d, ^2J = 15.2 Hz, 1H, CH$_2$), 1.51 (d, ^2J = 14.8 Hz, 1H, CH$_2$), 1.44 (s, 3H, ═CMe), 1.31 (s, 3H, CMe$_2$), 1.23 (d, *J* = 6.4 Hz, 3H, CHMe$_2$), 1.19 (d, *J* = 6.0 Hz, 3H, CHMe$_2$), 1.17 (s, 3H, CMe$_2$), 1.10 (d, *J* = 6.4 Hz, 3H, CHMe$_2$), 0.80 (d, *J* = 6.0 Hz, 3H, CHMe$_2$). ^{19}F NMR (CD$_2$Cl$_2$, 23 °C): δ −132.2 (d, *J* = 22.6 Hz, 6F, *o*-F), −163.0 (t, *J* = 20.3 Hz, 3F, *p*-F), −165.9 (m, 6F, *m*-F). ^{13}C NMR (CD$_2$Cl$_2$, 23 °C): δ 191.1 [C-(O^{i}Pr)═O], 155.5 [OC(O^{i}Pr)═], 134.6, 134.5, 131.9, 131.7, 131.6, 130.4, 130.0, 129.8, 129.7, 129.6, 128.4, 128.2, 126.5, 124.9, 124.6, 124.2, 124.1, 123.7, 122.7, 115.7, 111.9, 104.4, 66.56 (a total of 23 resonances observed for the Flu, Ph, C$_6$F$_5$, and Cp carbons; broad resonances for the C$_6$F$_5$ groups due to C−F coupling omitted), 86.22 (═CMe), 76.27, 68.73 (CHMe$_2$), 45.73 (CMe$_2$), 39.67 (CH$_2$), 24.60 (CMe$_2$), 22.22, 21.71, 21.11, 20.98 (CHMe$_2$), 18.71 (CMe$_2$), 17.26 (═CMe). ^{11}B NMR (CD$_2$Cl$_2$, 23 °C): δ −25.7 (d, $^1J_{B-H}$ = 89.8 Hz).

{[Me$_2$Si(Cp)(Flu)]Zr[OC(O^{i}Pr)═CMeCH$_2$C(Me$_2$)C(O^{i}Pr)═O]}$^+$[HB-(C$_6$F$_5$)$_3$]$^-$ (**9**). In situ generation and isolation of orange chelate **9** were carried out in the same manner as described for complex **1**. Anal. Calcd for $C_{52}H_{44}BO_4F_{15}SiZr$: C, 54.40; H, 3.86. Found: C, 54.30; H, 4.14.

*^{1}H NMR (CD$_2$Cl$_2$, 23 °C) for **9**.* δ 8.26−8.24 (m, 1H, Flu), 8.14 (d, *J* = 8.4 Hz, 1H, Flu), 7.74−7.70 (m, 2H, Flu), 7.62 (t, *J* = 7.6 Hz, 1H, Flu), 7.50−7.48 (m, 2H, Flu), 7.45 (t, *J* = 7.6 1H, Flu), 6.77 (q, *J* = 2.0 Hz, 1H, Cp), 5.95 (q, *J* = 2.5 Hz, 1H, Cp), 5.85 (q, *J* = 2.4 Hz, 1H, Cp), 5.77 (q, *J* = 2.0 Hz, 1H, Cp), 4.19 (sept, *J* = 6.2 Hz, 1H, CHMe$_2$), 3.89 (s, br, 1H, BH), 3.35 (sept, *J* = 6.2 Hz, 1H, CHMe$_2$), 2.30 (d, ^2J = 15.2 Hz, 1H, CH$_2$), 1.53 (d, ^2J = 14.8 Hz, 1H, CH$_2$), 1.45 (s, 3H, ═CMe), 1.32 (s, 3H, CMe$_2$), 1.28 (s, 3H, SiMe), 1.27 (d, *J* = 4.8 Hz, 3H, CHMe$_2$), 1.25 (d, *J* = 7.6 Hz, 3H, CHMe$_2$), 1.24 (s, 3H, SiMe), 1.17 (s, 3H, CMe$_2$), 1.14 (d, *J* = 6.4 Hz, 3H, CHMe$_2$), 0.86 (d, *J* = 6.0 Hz, 3H, CHMe$_2$). ^{19}F NMR (CD$_2$Cl$_2$, 23 °C): δ −132.1 (bs, 6F, *o*-F), −162.9 (bs, 3F, *p*-F), −165.7 (bs, 6F, *m*-F). ^{13}C NMR (CD$_2$Cl$_2$, 23 °C): δ 191.6 [C(O^{i}Pr)═O], 155.9 [OC(O^{i}Pr)═], 130.9, 130.2, 130.1, 129.8, 129.3, 128.5, 128.3, 126.5, 125.2, 125.0, 123.8, 123.7, 122.8, 114.7, 110.8, 108.6, 69.74 (a total of 17 resonances observed for the Flu, Ph, C$_6$F$_5$, and Cp carbons; broad resonances for the C$_6$F$_5$ groups due to C−F coupling omitted), 86.47 (═CMe), 76.68, 69.10 (CHMe$_2$), 45.86 (CMe$_2$), 40.14 (CH$_2$), 31.76 (CMe$_2$), 24.84 (CMe$_2$), 22.58, 22.00, 21.45 (CHMe$_2$), 17.61 (═CMe), −0.84, −0.89. ^{11}B NMR (CD$_2$Cl$_2$, 23 °C): δ −25.5 (d, $^1J_{B-H}$ = 89.8 Hz).

{rac-(EBI)Zr[OC(O^{i}Pr)═CMeCH$_2$C(Me$_2$)C(O^{i}Pr)═O]}$^+$[HB(C$_6$F$_5$)$_3$]$^-$ (**10**). The reaction of *rac*-(EBI)Zr[OC(O^{i}Pr)═CMe$_2$]$_2$ and B(C$_6$F$_5$)$_3$ was described previously,[12c] but the structure of the product was incorrectly assigned to be a borane-electrophilic-addition product, following the pathway established for the reaction of zirconocene ketone enolates with B(C$_6$F$_5$)$_3$ (vide supra). More detailed spectroscopic analysis, especially through coupled and decoupled ^{11}B NMR analysis, conclusively showed the reaction also proceeds through vinylogous hydride abstraction as demonstrated for other metallocene bis(ester enolate)s and thus forms the similar chelate product (i.e., **10**). Anal. Calcd for $C_{52}H_{42}BF_{15}O_4Zr$: C, 55.87; H, 3.79. Found: C, 55.85; H, 3.60.

*^{1}H NMR (CD$_2$Cl$_2$, 23 °C) for **10**.* δ 8.06 (d, *J* = 8.8 Hz, 1H), 7.92 (d, *J* = 8.8 Hz, 1H), 7.38−7.21 (m, 6H), 6.29 (d, *J* = 3.2 Hz, 3H), 5.97 (bs, 1H), 4.32 (sept, *J* = 6.0 Hz, 1H, CHMe$_2$), 4.13−3.93 (m, 4H, CH$_2$CH$_2$), 3.62 (m, br, 1H, BH), 3.62 (s, br, 1H, CHMe$_2$), 2.23 (bs, 1H, CH$_2$), 1.63 (bs, 1H, CH$_2$), 1.54 (s, 3H, ═CMe$_2$), 1.39 (d, *J* = 6.0 Hz, 3H, CHMe$_2$), 1.28 (d, *J* = 6.0 Hz, 3H, CHMe$_2$), 1.21 [bs, 9H, *Me*'s for CHMe$_2$ (3H), and CMe$_2$ (6H)], 1.01 (bs, 3H, CHMe$_2$). ^{13}C NMR (CD$_2$Cl$_2$, 23 °C, only key resonances shown): δ 192.8 [C(O^{i}Pr)═O], 155.2 [OC(O^{i}Pr)═], 86.68 (═CMe), 77.29, 69.39 (CHMe$_2$), 44.01 (CMe$_2$), 40.43 (CH$_2$), 30.89 (CMe$_2$), 30.67, 29.34 (CH$_2$CH$_2$), 24.83 (CMe$_2$), 22.66, 22.26, 21.96, 21.21 (CHMe$_2$), 17.92 (═CMe). ^{19}F NMR (CD$_2$Cl$_2$, 21 °C): δ −132.3 (bs, 6F, *o*-F), −163.0 (bs, 3F, *p*-F), −165.8 (bs, 6F, *m*-F). ^{11}B NMR (CD$_2$Cl$_2$, 23 °C): δ −25.6 (d, $^1J_{B-H}$ = 89.8 Hz).

{(CGC)Zr[OC(O^{i}Pr)═CMeCH$_2$C(Me$_2$)C(O^{i}Pr)═O]}$^+$[HB(C$_6$F$_5$)$_3$]$^-$ (**11**). The NMR-scale reaction of (CGC)Zr[OC(O^{i}Pr)═CMe$_2$]$_2$ and B(C$_6$F$_5$)$_3$ in CD$_2$Cl$_2$ was described previously,[12a] but the structure of the product was incorrectly assigned to be a borane-electrophilic-addition product (vide supra). More detailed spectroscopic analysis and isolation now conclusively showed the reaction also proceeds through vinylogous hydride abstraction and forms the similar chelate product **11** as a yellow solid in quantitative yield. Anal. Calcd for $C_{47}H_{53}BF_{15}O_4SiNZr$: C, 50.81; H, 4.81; N, 1.26. Found: C, 51.07; H, 5.08; N, 1.21.

*^{1}H NMR (CD$_2$Cl$_2$, 23 °C) for **11**.* δ 5.24 (sept, *J* = 6.3 Hz, 1H, CHMe$_2$), 4.30 (sept, *J* = 6.0 Hz, 1H, CHMe$_2$), 3.57 (q, *J* = 90.7 Hz, 1H, BH), 2.23 (s, 3H, C$_5$Me$_4$), 2.22 (s, 3H, C$_5$Me$_4$), 2.10 (s, 3H, C$_5$Me$_4$), 1.99 (s, 3H, C$_5$Me$_4$), 1.62 (s, 2H, ═CH$_2$), 1.47 (d, *J* = 6.3 Hz, 3H, CHMe$_2$), 1.44 (d, *J* = 6.0 Hz, 3H, CHMe$_2$), 1.41 (s, 3H, ═CMe), 1.34 (s, 3H, CMe$_2$), 1.274 (d, *J* = 5.7 Hz, 3H, CHMe$_2$), 1.265 (s, 3H, CMe$_2$), 1.21 (d, *J* = 6.3 Hz, 3H, CHMe$_2$), 1.17 (s, 9H, NCMe$_3$), 0.73 (s, 3H, SiMe$_2$), 0.66 (s, 3H, SiMe$_2$). ^{19}F NMR (CD$_2$Cl$_2$, 23 °C): δ −132.2 (d, J_{F-F} = 22.3 Hz, 6F, *o*-F), −163.1 (t, J_{F-F} = 20.3 Hz, 3F, *p*-F), −165.9 (m, 6F, *m*-F). ^{13}C NMR (CD$_2$Cl$_2$, 23 °C): δ 193.8 [C(O^{i}Pr)═O], 159.3 [OC(O^{i}Pr)═], 135.9, 133.5, 132.7, 130.8,

108.3 (a total of five resonances observed for the Cp carbons; broad resonances for the C_6F_5 groups due to C−F coupling omitted), 79.70, 70.88, 58.17, 45.35, 41.63, 34.09, 33.91, 31.07, 25.42, 22.97, 22.37, 21.73, 21.64 ($CHMe_2$), 17.38 (=CMe), 14.08, 13.95, 12.33, 11.20 ($CpMe_4$), 7.19, 5.85 ($SiMe_2$). ^{11}B NMR (CD_2Cl_2, 23 °C): δ −25.6 (d, $^1J_{B-H}$ = 89.8 Hz).

{$Cp_2Zr[OC(O^iPr)$=$CMeCH_2C(Me_2)C(O^iPr)$=$O]$}$^+$[$HB(C_6F_5)_3$]$^-$ (**12**). The reaction of $Cp_2Zr[OC(O^iPr)$=$CMe_2]_2$ and $B(C_6F_5)_3$ was described previously,[12b] but the structure of the product was incorrectly assigned to be a borane-electrophilic-addition product. More detailed spectroscopic analysis, especially through coupled and decoupled ^{11}B NMR analysis, conclusively showed the reaction also proceeds through vinylogous hydride abstraction and forms the chelate **12** as a red oil. Anal. Calcd for $C_{42}H_{36}BO_4F_{15}Zr$: C, 50.87; H, 3.66. Found: C, 49.99; H, 3.27.

^{1}H NMR (CD_2Cl_2, 23 °C) for **12**. δ 6.57 (s, 10H, C_5H_5), 4.98 (sept, J = 6.3 Hz, 1H, $CHMe_2$), 4.09 (sept, J = 6.3 Hz, 1H, $CHMe_2$), 3.62 (s, br, 1H, B*H*), 2.31 (bs, 2H, CH_2), 1.67 (s, 3H, =CMe_2), 1.43 (d, J = 6.3 Hz, 6H, $CHMe_2$), 1.39 (s, 6H, CMe_2), 1.20 (d, J = 6.3 Hz, 6H, $CHMe_2$). ^{19}F NMR (CD_2Cl_2, 23 °C): δ −132.1 (d, J_{F-F} = 22.3 Hz, 6F, *o*-F), −162.7 (t, J_{F-F} = 19.6 Hz, 3F, *p*-F), −165.6 (m, 6F, *m*-F). ^{13}C NMR (CD_2Cl_2, 23 °C): δ 193.6 [$C(O^iPr)$=O], 155.9 [$OC(O^iPr)$=], 117.5, 115.5, 115.4, 114.6, 114.1 (a total of five resonances observed for the Cp carbons; broad resonances for the C_6F_5 groups due to C−F coupling omitted), 88.68 (=*C*Me), 77.59, 70.37 (*C*HMe$_2$), 45.42 (*C*Me$_2$), 40.81 (CH_2), 27.49 (CMe_2), 22.24, 21.80 ($CHMe_2$), 17.90 (=CMe). ^{11}B NMR (CD_2Cl_2, 23 °C): δ −25.4 (d, $^1J_{B-H}$ = 89.8 Hz).

General Polymerization Procedures. MMA polymerizations were performed either in 25 mL flame-dried Schlenk flasks interfaced to the dual-manifold Schlenk line for runs using external temperature bath or in 30 mL glass reactors inside the glovebox for ambient temperature (ca. 25 °C) runs. Two different activation procedures were employed for comparative studies. In a in-reactor activation procedure (mostly for activated species that are unstable in the absence of monomer), a predetermined amount (equimolar to the catalyst precursor) of a suitable activator such as $[Ph_3C][B(C_6F_5)_4]$, THF·$B(C_6F_5)_3$, $B(C_6F_5)_3$, or $[H(Et_2O)_2][B(C_6F_5)_4]$ was first dissolved in MMA (1.00 mL, 9.35 mmol) and 5 mL of solvent (CH_2Cl_2 or toluene) inside a glovebox, and the polymerization was started by rapid addition of a solution of a precatalyst (23.4 μmol, for a run with a [MMA]:[catalyst] of 400:1 ratio) in 4 mL of solvent (CH_2Cl_2 or toluene) via a gastight syringe to the above activator + MMA solution under vigorous stirring at the pre-equilibrated bath temperature. The amount of the MMA was fixed for all polymerizations, whereas the amount of the catalyst was adjusted according to the [MMA]:[Zr] ratio specified in the text. In a preactivation procedure (mostly for activated species that are stable in the absence of monomer), a precatalyst was premixed with an appropriate activator in solution for 10 min to generate the corresponding activated species, followed by rapid addition of MMA to start the polymerization. In both activation procedures, after the measured time interval, a 0.2 mL aliquot was taken from the reaction mixture via syringe and quickly quenched into a 4 mL vial containing 0.6 mL of undried "wet" $CDCl_3$ stabilized by 250 ppm of BHT-H; the quenched aliquots were later analyzed by ^{1}H NMR to obtain the percent monomer conversion data. The polymerization was immediately quenched after the removal of the aliquot by addition of 5 mL of 5% HCl-acidified methanol. The quenched mixture was precipitated into 100 mL of methanol, stirred for 1 h, filtered, washed with methanol, and dried in a vacuum oven at 50 °C overnight to a constant weight.

Polymerization Kinetics. Kinetic experiments were carried out in a stirred glass reactor at ambient temperature (ca. 25 °C) inside an argon-filled glovebox using the in-reactor activation procedure already described above and with $[MMA]_0/[Zr]_0$ ratios of 100:1, 200:1, 400:1, 600:1, 800:1, and 1000:1, where $[MMA]_0$ = 0.935 M, $[Zr]_0$ = $[activator]_0$ = 9.35, 4.67, 2.34, 1.56, 1.17, and 0.935 mM in 10 mL of CH_2Cl_2 + MMA solutions. The procedures for obtaining the monomer conversion data versus reaction time were described in the literature.[5c,21] Specifically, at appropriate time intervals, 0.2 mL aliquots were withdrawn from the reaction mixture using syringe and quickly quenched into 1 mL septum-sealed vials containing 0.6 mL of undried "wet" $CDCl_3$ mixed with 250 ppm BHT-H. The quenched aliquots were analyzed by ^{1}H NMR. The ratio of $[MMA]_0$ to $[MMA]_t$ at a given time t, $[MMA]_0/[MMA]_t$, was determined by integration of the peaks for MMA (5.2 and 6.1 ppm for the vinyl signals; 3.4 ppm for the O*Me* signal) and PMMA (centered at 3.4 ppm for the O*Me* signals) according to $[MMA]_0/[MMA]_t = 2A_{3.4}/3A_{5.2+6.1}$, where $A_{3.4}$ is the total integrals for the peaks centered at 3.4 ppm (typically in the region 3.2−3.6 ppm) and $A_{5.2+6.1}$ is the total integrals for both peaks at 5.2 and 6.1 ppm. Apparent rate constants (k_{app}) were extracted by linearly fitting a line to the plot of $\ln([MMA]_0/[MMA]_t)$ versus time.

Polymerization Thermodynamics. Experiments for acquiring the polymerization thermodynamic parameters were carried out in an NMR tube at the appropriate temperature using the in-reactor activation procedure already described above and with a fixed $[MMA]_0$:$[catalyst]_0$ ratio of 100:1, where $[MMA]_0$ = 0.467 M and $[catalyst]_0$ = 4.67 mM in 1 mL of CD_2Cl_2 + MMA solutions. A selected example is described below. In an argon-filled glovebox, an NMR tube was charged with 4.0 mg (4.7 μmol) of $[Ph_2C(Cp)(2,7\text{-}^tBu_2\text{-}Flu)]Zr[OC(O^iPr)$=$CMe_2]_2$ and 0.05 mL of MMA in 0.5 mL of CD_2Cl_2. This NMR tube was sealed with a rubber septum, removed from the glovebox, and cooled to −78 °C. A 0.5 mL CD_2Cl_2 solution of $B(C_6F_5)_3$ (4.7 μmol) was slowly added to this tube via syringe. The reactions were monitored immediately by ^{1}H NMR at given temperature. The ratio of $[MMA]_0$ to $[MMA]_t$ at a given time t, $[MMA]_0/[MMA]_t$, was determined by integration of the peaks for MMA and PMMA according to the procedure already described above. Apparent rate constants (k_{app}) were extracted by linearly fitting a line to the plot of $\ln([MMA]_0/[MMA]_t)$ versus time. The activation enthalpy ($\Delta H^{\ddagger}$) and entropy ($\Delta S^{\ddagger}$) for the reaction were obtained according to the transition-state theory expression for the rate constant ($k = (k_BT/h)\exp(-\Delta H^{\ddagger}/RT)\exp(\Delta S^{\ddagger}/R)$. A plot of $\ln(hk/k_BT)$ versus $1/T$ gave a straight line, the slope and intercept of which yielded $\Delta H^{\ddagger}$ and $\Delta S^{\ddagger}$. The free activation energy ($\Delta G^{\ddagger}$) was calculated according to the equation $\Delta G^{\ddagger} = \Delta H^{\ddagger} - T\Delta S^{\ddagger}$ at a given temperature.

Polymer Characterizations. The isolated low MW PMMA sample was analyzed by matrix-assisted laser desorption/ionization time-of-flight mass spectroscopy (MALDI−TOF MS); the experiment was performed on an Ultraflex MALDI-TOF mass spectrometer (Bruker Daltonics) operated in positive ion, reflector mode using a Nd:YAG laser at 355 nm and 25 kV accelerating voltage. A thin layer of a 1% NaI solution was first deposited on the target plate, followed by 0.6 μL of both sample and matrix (dithranol, 10 mg/mL in 50% ACN, 0.1% TFA). External calibration was done using a peptide calibration mixture (4−6 peptides) on a spot adjacent to the sample. The raw data were processed in the FlexAnalysis software (version 2.4, Bruker Daltonics).

Polymer number-average molecular weights (M_n) and molecular weight distributions or polydispersity indices (PDI = M_w/M_n) were measured by gel permeation chromatography (GPC) analyses carried out at 40 °C and a flow rate of 1.0 mL/min, with $CHCl_3$ as the eluent on a Waters University 1500 GPC instrument equipped with one PLgel 5 μm guard and three PLgel 5 μm mixed-C columns (Polymer Laboratories; linear range of molecular weight = 200−2 000 000). The instrument was calibrated with 10 PMMA standards, and chromatograms were processed with Waters Empower software (version 2002). ^{1}H NMR and ^{13}C NMR spectra for the analysis of PMMA microstructures were recorded in $CDCl_3$ and analyzed according to the literature methods.[5c−5e,29]

Models and Computational Details. Calculations followed the procedures described in our prior publications.[30] Specifically, the Amsterdam Density Functional (ADF) program was used to obtain all the results.[31] The electronic configuration of the molecular systems was described by a triple-ζ STO basis set on Zr (ADF basis set TZV).[31a] Triple-ζ STO basis sets, augmented by one polarization function, were used for main group atoms (ADF basis sets TZVP).[31a] The inner shells on Zr (including 2p and 3d, respectively), Si (including 2p), B, C, N, O,

Scheme 1. Electrophilic Addition of $B(C_6F_5)_3$ to Ketone Enolates versus Vinylogous Hydride Abstraction of Ester Enolates by $B(C_6F_5)_3$

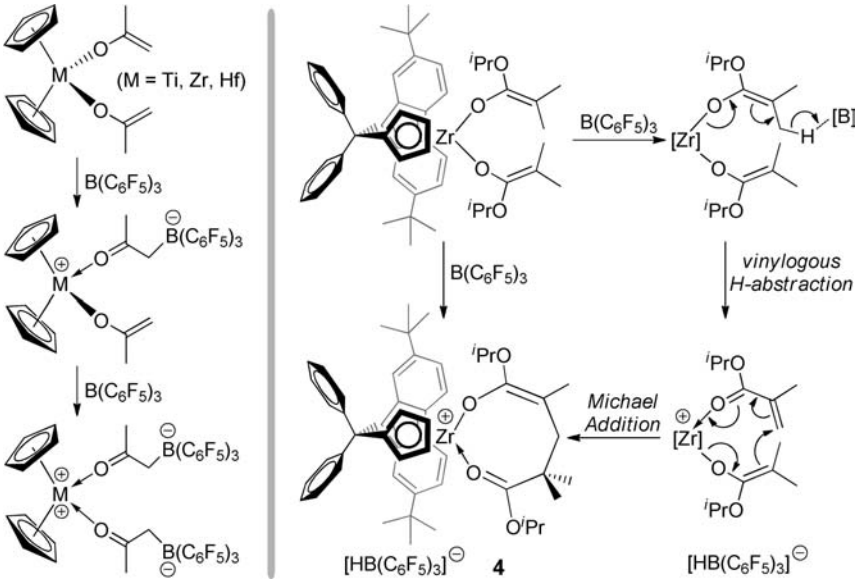

and F (1s) were treated within the frozen core approximation. Energies and geometries were evaluated using the local exchange-correlation potential by Vosko et al.,[32] augmented in a self-consistent manner with Becke's[33] exchange gradient correction and Perdew's[34] correlation gradient correction (BP86 functional). All geometries were localized in the gas phase. However, because the MMA polymerizations herein described have been performed in toluene and in a rather polar solvent, such as CH_2Cl_2, we performed single point energy calculations on the final geometries to take into account solvent effects. The ADF implementation of the conductor-like screening model (COSMO)[35] was used. A dielectric constant of 2.8 and a radius of 3.48 Å were used to represent toluene as the solvent, while a dielectric constant of 8.9 and a solvent radius of 2.94 Å were used to represent CH_2Cl_2 as the solvent. The following radii, in angstroms, were used for the atoms: H 1.16, C 2.00, O 1.50, Si 2.20, and Zr 2.40. All the reported energies included solvent effects.

RESULTS AND DISCUSSION

Activation of Bis(ester enolate) Complexes by $B(C_6F_5)_3$ to Cationic Metallacycles. Erker and co-workers established that the reaction of group IV metallocene bis(ketone enolate)s with $B(C_6F_5)_3$ forms direct adducts via electrophilic addition of the borane to the nucleophilic enolate carbon center (Scheme 1, left column).[15] On the other hand, we recently found that the reaction of $B(C_6F_5)_3$ with a C_s-ligated *ansa*-zirconocene bis(ester enolate) complex, which is sterically protected at nucleophilic α-carbon of the enolate ligand by two methyl groups, affords cleanly at room temperature the cationic eight-membered chelate **4** (Scheme 1, right column).[14] This activation can be reasoned to proceed through vinylogous hydride abstraction from the Me group of the enolate $[OC(O^iPr)=CMe_2]$ moiety by $B(C_6F_5)_3$ to form the anion $[HB(C_6F_5)_3]^-$ and the resulting isopropyl methacrylate coordinated to Zr; subsequent nucleophilic addition of the second enolate ligand on Zr to this coordinated isopropyl methacrylate produces the cationic eight-membered chelate (Scheme 1, right column). This ion pair exhibits spectroscopic signatures for (a) the uncoordinated $[HB(C_6F_5)_3]^-$ anion[36,37] [B*H* at 3.60 ppm (q, ^1J = 91.6 Hz) in the ^{1}H NMR spectrum, a small chemical shift difference between the *para*- and *meta*-fluorines in the ^{19}F NMR spectrum, $\Delta(m,p\text{-F})$ = 2.5 ppm) for B−C$_6$*F*$_5$,[38] and a *B*H doublet at −25.4 ppm ($^1J_{B-H}$ = 93.7 Hz) in the ^{11}B NMR spectrum], and (b) cationic eight-membered chelates[5] (one of which was structurally characterized[12c]) [most notably two diastereotopic C*H*$_2$ protons at 2.44 (d) and 1.58 (d) as well as coexistence of both the datively bound ester chain end (δ 4.26, sept. for OC*H*Me$_2$ in ^{1}H NMR and δ 190.7 for C(O^iPr)= O in ^{13}C NMR) and the covalently bound ester enolate (δ 3.31, sept. for OC*H*Me$_2$ and δ 155.8 for OC(O^iPr)=) entities].

Considering the importance of such a cationic chelating structure, which simulates the active propagating species (resting state) in the methacrylate polymerization,[1] the ease of its one-step generation, and its remarkable thermal stability enabling its isolation at room temperature (cf. the active species derived from activation by $[Ph_3C][B(C_6F_5)_4]$ and $[H(Et_2O)_2][B(C_6F_5)_4]$ is a mixture containing chelate and nonchelate species and an ester-coordinated nonchelate species, respectively,[14] which is unstable at room temperature in the absence of monomer), we were attracted to investigate if this activation methodology can be extended to other types of group IV metallocene bis(ester enolate) precatalysts or not. Gratifyingly, we found that this activation methodology is remarkably general, which readily produces cationic eight-membered-ring chelates **1**−**12** (Chart 1) in quantitative yields at room temperature, from the corresponding group IV metallocene bis(ester enolate) precursors that varied metals, bridging atoms, substituents, substitution patterns, and ligand symmetries. All these cationic chelating complexes exhibit similar spectroscopic characteristics (vide supra; see also Experimental Section) for the cationic eight-membered metallacycles paired with the uncoordinated $[HB(C_6F_5)_3]^-$ anion. Most notably, their ^{11}B (CD_2Cl_2, 23 °C: δ from −25.7 to −25.4, d, $^1J_{B-H}$ = 94−88 Hz) and ^{19}F (CD_2Cl_2, 23 °C: δ −132 (d, 6F, *o*-F), −163 (t, 3F, *p*-F), −166 (m, 6F, *m*-F) NMR spectra (Figure 1) are essentially identical for all the complexes, due to the presence of the same uncoordinated hydridoborate anion.

We also investigated the energetics of activation of the bis(enolate) complex of **1** by $B(C_6F_5)_3$ computationally (Scheme 2).

dx.doi.org/10.1021/ja109775v |*J. Am. Chem. Soc.* 2011, 133, 1572–1588

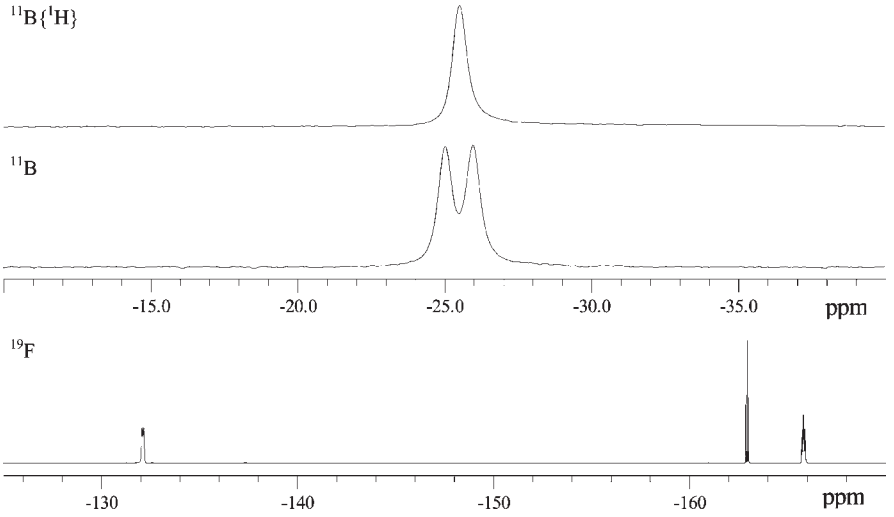

Figure 1. ^{11}B NMR spectra (CD_2Cl_2, 23 °C; top, $^{11}B\{^1H\}$ decoupled; middle, coupled) and ^{19}F NMR spectrum (CD_2Cl_2, 23 °C) of **1**.

Scheme 2. Energetics (kcal/mol) Involved in the Bis(enolate) Activation by $B(C_6F_5)_3$ to Form 1, Relative to the Reference State of 0 kcal/mol for the Starting Bis(enolate) Complex[a]

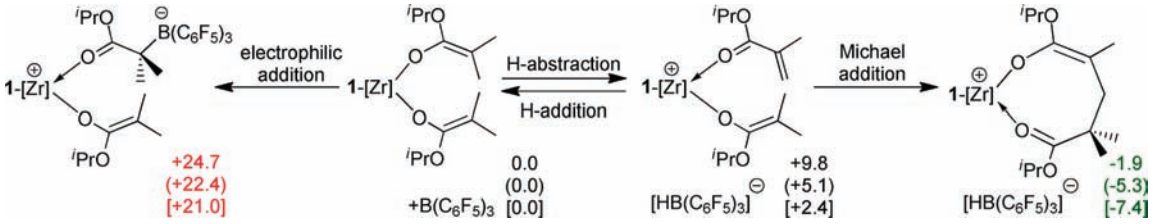

[a] Values are reported without parentheses for gas phase, in round parentheses (toluene), and in square brackets [CH_2Cl_2].

Calculations indicate that initial hydride-abstraction to form the monoenolate intermediate is slightly endothermic. Due to the formation of charged species, polar solvents stabilize this intermediate. Michael addition of the remaining enolate ligand to the formed methacrylate leads to the eight-membered chelate species, which is the most stable species also in the gas phase and further stabilized by solvent effects for this charge separated chelate.

As to the possible competing pathway, formation of the borane adduct via electrophilic addition of the borane to the nucleophilic ester enolate carbon center, our computational results show that the adduct, whatever solvent is considered, is calculated to be more than 20 kcal/mol higher in energy relative to the starting bis(enolate) species (Scheme 2), consistent with hydride abstraction product formation observed experimentally (vide supra). Significantly, these calculations also pointed to the reversibility of this activation in the hydride abstraction step. In fact, the abstracted hydride in $[HB(C_6F_5)_3]^-$ can be reversibly donated to the methacrylate coordinated to the Zr center, thus providing a theoretical ground for a hydride-shuttling chain-transfer mechanism (vide infra).

Characteristics of Polymerization by Catalysts 1−12. The MMA polymerization by catalysts **1−12** was investigated to uncover the following polymerization characteristics: catalyst activity (TOF), polymerization efficiency (I^*), polymer MW (M_n and MWD), and polymer tacticity (methyl triads, %rr, %mr, and %mm). In these comparative polymerization studies, we fixed the [MMA]:[catalyst] ratio to be 400:1 (and MMA and catalyst concentrations) as well as polymerization temperature (room temperature) and medium (CH_2Cl_2). We first compared

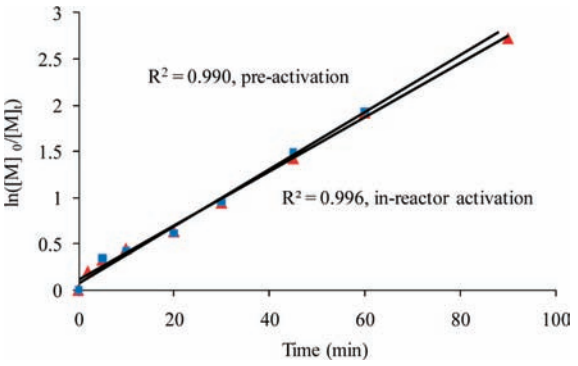

Figure 2. Plots of the first-order kinetics of $\ln([MMA]_0/[MMA]_t)$ versus time (min) for the polymerization of MMA by $[Ph_2C(Cp)(2\text{-}^t\text{Bu}-\text{Flu})]Zr[OC(O^i\text{Pr})=CMe_2]_2$ activated with equimolar $B(C_6F_5)_3$ in CH_2Cl_2 at 25 °C. Conditions: $[MMA]_0$ = 0.935 M; $[Zr]_0$ = 2.34 mM; preactivation method (blue ■) versus in-reactor activation method (red ▲).

the polymerizations using a given precatalyst subjected to the preactivation and the in-reactor activation methodology (see Experimental Section) and found that the MMA polymerizations in CH_2Cl_2 at room temperature by $[Ph_2C(Cp)(2\text{-}^t\text{Bu}-\text{Flu})]Zr[OC(O^i\text{Pr})=CMe_2]_2$ activated with equimolar $B(C_6F_5)_3$ via preactivation and in-reactor activation gave nearly superimposable first-order kinetic profiles (Figure 2). Thus, considering relative convenience of the procedure and goodness of fit to the first-order kinetic plot, the in-reactor activation methodology

dx.doi.org/10.1021/ja109775v |*J. Am. Chem. Soc.* 2011, 133, 1572–1588

Table 1. Results of MMA Polymerization by Catalysts 1−12 [a]

run no.	catalyst	time (h)	conv.[b] (%)	TOF (h^{-1})	$10^{-3}M_n$[c] (g/mol)	MWD[c] (M_w/M_n)	I^*[d] (%)	[rr][b] (%)	[mr][b] (%)	[mm][b] (%)
1	**1** (Zr)	24	94.8	16	21.0	1.39	182	87.0	11.8	1.2
2	**2** (Ti)	24	59.6	10	5.78	1.50	418	72.7	25.5	1.8
3	**3** (Hf)	24	7.2	1	bimodal	bimodal	N.A.	80.4	16.0	3.6
4	**4**	1.5	97.2	260	40.1	1.39	97.8	90.5	7.7	1.8
5	**4** (tol)	24	95.4	16	17.7	1.63	218	87.5	10.6	1.9
6	**5**	2.4	97.2	162	21.3	1.40	184	85.6	12.3	2.1
7	**5** (tol)	24	66.8	11	16.7	1.65	162	85.4	12.3	2.4
8	**6**	27	21.9	3	4.10	1.31	220	77.5	20.7	1.8
9	**7**	2	98.1	196	34.1	1.39	116	90.5	7.6	1.9
10	**8** (tol)	24	26.6	1	2.52	1.33	116	62.5	27.1	10.4
11	**9**	24	0	0						
12	**10**	1	98.4	394	107	1.06	37	2.1	4.6	93.3
13	**11**	24	25.4	4	8.28	1.56	126	73.5	24.8	1.7
14	**12**	24	100	17	3.11	1.36	1300	65.6	32.5	1.9

[a] Carried out at ambient temperature (~25 °C) in 9 mL of CH_2Cl_2 (unless toluene (tol) was indicated) and 1 mL of MMA solutions, where $[MMA]_0$ = 0.935 M and $[precatalyst]_0 = [B(C_6F_5)_3]_0$ = 2.34 mM for a [MMA]:[catalyst] ratio of 400:1, except for run 10 where a 100:1 ratio was used. [b] Monomer conversions and PMMA methyl triad distributions measured by ^1H NMR. [c] M_n and MWD determined by GPC relative to PMMA standards. [d] Initiator efficiency (I^*) = M_n(calcd)/M_n(exptl), where M_n(calcd) = MW(MMA) × $[MMA]_0/[cat]_0$ × conversion % + MW of chain-end groups (258).

was employed for all the polymerization studies described herein, the results of which are summarized in Table 1.

Supported by *ansa*-Flu-Cp ligands, catalysts **1**−**9** varied metals, bridging atoms, substituents, and substitution patterns, each of which variation impacts the polymerization characteristics in different degrees. First, with the $[Ph_2C(Cp)(Flu)]$ ligand fixed, Zr catalyst **1** is most active (16 h^{-1} TOF, run 1), Ti catalyst **2** lies in the middle (10 h^{-1} TOF, run 2), while Hf catalyst **3** is least active (1 h^{-1} TOF, run 3). The polymers produced by **1** and **2** have measured M_n's being much lower than the calculated values, thus giving much-greater-than-100% I^*'s, characteristics of a polymerization system with a significant degree of chain transfer. Zirconium catalyst **1** also produces *st*-PMMA with the highest syndiotacticity (87% rr) among these three catalysts. However, even Zr catalyst **1** exhibits a much lower activity, a tendency to chain-transfer (182% I^*), and a noticeably lower syndiotacticity, as compared to the same cation, but paired with more commonly used weakly coordinating anions $[MeB(C_6F_5)_3]^-$ (800 h^{-1} TOF, 48% I^*, 94% rr) and $[B(C_6F_5)_4]^-$ (717 h^{-1} TOF, 41% I^*, 94% rr)[14] under the same polymerization conditions. Intuitively, the much lower activity observed for the catalyst paired with the anion $[HB(C_6F_5)_3]^-$ may be related to its possibly stronger ion-pairing that impedes monomer coordination. However, this level of anion modulation on the MMA polymerization syndiospecificity was not anticipated, as the cation in this type of catalyst is the eight-membered resting active intermediate, which simulates the structure of the active propagating species, and as our prior study[14] showed negligible anion effect on the resulting PMMA syndiotacticity with the same cation, but paired with different weakly coordinating anions including $[MeB(C_6F_5)_3]^-$, $[B(C_6F_5)_4]^-$, and $[TRISPHAT]^-$. On the other hand, Erker and co-workers[4d] provided evidence for active involvement of anion (i.e., in the transition state of the conjugate addition step) in the polymerization activity and stereoselectivity while examining MMA polymerization characteristics using a series of alkyl-substituted, $Me_2Si<$ bridged bis(Cp) cationic complexes paired with different anions, $[MeB(C_6F_5)_3]^-$ versus the pendent oligomeric anion $[PMMA-C_4H_6-MeB(C_6F_5)_3]^-$.

Second, substituting the Flu ring at 2,7-positions with ^{t}Bu (catalyst **4**, run 4) drastically increases the polymerization activity (by 16-fold, TOF = 260 h^{-1}) and the degree of polymerization control (now with a nearly quantitative I^* of 98%; run 4 vs run 1), coupled with a much smaller, but nonetheless noticeable, increase in syndiotacticity of the resulting PMMA (90.5% rr by **4** vs 87% rr by **1**). The same activity trend was also observed for the $[Ph_3C][B(C_6F_5)_4]$ activated polymerization system, which was attributed to the calculated lower backbiting and much lower ion-pairing energies for the 2,7-^{t}Bu$_2$-substituted cation as compared to the unsubstituted one, but the syndiospecificity of the cation paired with the anion $[B(C_6F_5)_4]^-$ remains unchanged before and after the ^{t}Bu substitution.[14] In sharp contrast to the insensitivity of activity and syndiotacticity of the $[MeB(C_6F_5)_3]^-$- and $[B(C_6F_5)_4]^-$-based catalysts to solvent polarity,[14] activity of catalyst **4** was dramatically reduced by 16-fold on going from CH_2Cl_2 (ε = 8.93; run 4) to toluene (ε = 2.38; run 5); the polymerization in toluene also exhibited significant chain transfer (218% I^*) and produced PMMA with a somewhat lower syndiotacticity (87.5% rr). Removing one of the two ^{t}Bu groups from the Flu ring produced less active (162 h^{-1} TOF), more efficient (184% I^*), and less syndiospecific (85.6% rr) catalyst **5** (run 6), but it is still far more active than catalyst **1** without any substitution on the Flu ring (run 1). Again, catalyst **5** with the anion $[HB(C_6F_5)_3]^-$ is noticeably less syndiospecific than the same cation paired with $[B(C_6F_5)_4]^-$ (92.3% rr), and the polymerization in toluene is much slower (by 15-fold) than the one carried out in CH_2Cl_2, while the I^* value was similar and the polymer syndiotacticity remained the same (run 7 vs run 6). Placing a ^{t}Bu group on the Cp ring instead of the Flu ring resulted in catalyst **6** with only marginal activity (3 h^{-1} TOF, run 8) and modest syndioselectivity (77.5% rr).

Third, while examining potential electronic effects of the bridging aryl groups on polymerization, we found that catalyst **7** with the silyl group (Et_3Si) substituted on the *para*-Ph ring performs similarly to catalyst **4** in both polymerization activity and polymer syndiotacticity (run 9 vs run 4), consistent with the observed nearly identical polymerization performance for these two cations paired with the anion $[B(C_6F_5)_4]^-$.[14] On the other hand, placing a silyl group at the bridge either completely shuts down the polymerization with the $Me_2Si<$ bridge (**9**, run 11) or renders a catalyst with the $Ph_2Si<$ bridge (**8**, run 10) exhibiting

dx.doi.org/10.1021/ja109775v | J. Am. Chem. Soc. 2011, 133, 1572–1588

Table 2. Selected MMA Polymerization Results by Catalyst 4 in CH_2Cl_2 at 25 °C[a]

run no.	[MMA] (mol/L)	[MMA]/[4]	time (h)	conv. (%)	$10^{-3}M_n$ (g/mol)	MWD (M_w/M_n)	I^* (%)	[rr] (%)	[mr] (%)	[mm] (%)
15	0.935	100	0.25	96.5	11.3	1.48	87.8	87.7	8.7	3.6
16	0.935	200	1	100	25.6	1.24	79.2	89.8	8.1	2.1
17	0.935	400	1.5	97.2	40.1	1.39	97.8	90.5	7.7	1.8
18	0.935	600	4	98.0	40.8	1.49	145	90.3	8.0	1.7
19	0.935	800	4	95.2	44.7	1.75	170	89.4	8.7	1.9
20	0.935	1000	5	92.7	48.3	1.73	193	89.5	8.8	1.7

[a] See footnotes in Table 1 for explanation of abbreviations.

only marginal activity (1 h^{-1} TOF) and low syndioselectivity (62.5% rr). Last, $[HB(C_6F_5)_3]^-$-based catalysts with C_2-ligation (**10**, run 12), C_s (constrained geometry)-ligation (**11**, run 13), and C_{2v}-ligation (**12**, run 14) appeared to produce PMMA with tacticity similar to the polymer produced by the same cation but paired with other weakly coordinating anions.[1]

Overall, the MMA polymerization by the eight-membered chelating cations supported by C_s-*ansa*-Flu-Cp ligands is quite sensitive to inclusion of a hydride to the anion structure. For such cations paired with a weakly coordinating anion, such as $[MeB(C_6F_5)_3]^-$, $[B(C_6F_5)_4]^-$, or $[TRISPHAT]^-$, their high polymerization activity and high syndiospecificity are not noticeably affected by these three anion structures and solvent polarity (between toluene and CH_2Cl_2). However, an exception seems to be the cations paired with the hydridoborate anion $[HB(C_6F_5)_3]^-$, as such catalysts produce PMMA with noticeably lower syndiotacticity (by 4−7% rr) and significantly lower activity (by 6−40-fold), when compared to the same cations paired with those more commonly used weakly coordinating anions. Additionally, $[HB(C_6F_5)_3]^-$-based catalysts have experienced drastic activity differences in different solvents, with the activity in toluene being ~16-fold lower than that in CH_2Cl_2. Most intriguingly, $[HB(C_6F_5)_3]^-$-based catalysts have enabled significant internal (i.e., without addition of chain-transfer reagents) chain-transfer reaction, especially for the cations without 2,7-substituents on the Flu ring (**1**, **2**, **5**, and **6**) or the cation with such substituents (**4**) in the toluene medium. For structurally similar, $Ph_2C<$ bridged Flu-Cp type catalysts, there seems to be a rather general trend: catalysts under conditions that promote more significant chain-transfer reactions produce polymers with lower syndiotacticity. (Monitoring the polymer tacticity versus monomer conversion for selected catalyst systems **4** and **12** revealed that the stereoselectivity remained essentially constant from low to high monomer conversions, thus ensuring that the nature of the active species does not change over the polymerization course.) Further discussions on these interesting observations will be made in the computational section.

Kinetics of Polymerization by Catalyst 4. As Zr cation **4** generated by the in-reactor activation of its bis(ester enolate) precursor with $B(C_6F_5)_3$ is the most active, efficient, and syndiospecific catalyst within this series, we subsequently examined the MMA polymerization by this catalyst in more detail, specifically concerning its degree of control and kinetics of polymerization. Noteworthy is that a much more active polymerization system can be generated by activation with 2 equiv of $Al(C_6F_5)_3$, which achieved a quantitative monomer conversion in 10 min at room temperature to give a high TOF of 2400 h^{-1} and produced PMMA with $M_n = 7.31 \times 10^4$, $M_w/M_n = 1.15$; however, the polymerization by metallocene bis(ester enolate)s activated with $Al(C_6F_5)_3$ proceeds through formation of enolaluminate intermediates,[10] thus producing PMMA with a considerably lower syndiotacticity (73.2% rr).

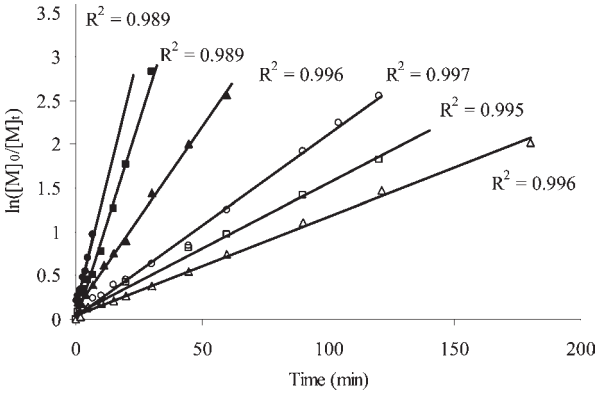

Figure 3. Plots of the first-order kinetics of $\ln([MMA]_0/[MMA]_t)$ versus time (min) for the MMA polymerization by catalyst **4** in CH_2Cl_2 at 25 °C. Conditions: $[MMA]_0 = 0.935$ M; $[Zr]_0 = 9.35$ (●), 4.67 (■), 2.34 (▲), 1.56 (○), 1.17 (□), and 0.935 (△) mM.

Table 2 summarizes the MMA polymerization results with varied $[MMA]_0/[4]_0$ ratios by 10-fold (from 100 to 1000) in CH_2Cl_2 at room temperature. As can be seen from this table, there was an initial linear response of the polymer M_n to an increase in the $[MMA]_0/[4]_0$ ratio from 100 (run 15) to 200 (run 16) and to 400 (run 17), but further increasing the ratio to 600 (run 18) to 800 (run 19) and to 1000 (run 20) did not result in an increase in M_n of PMMA corresponding to those ratios. It is clear that the degree of the control of the polymerizations at high $[MMA]_0/[4]_0$ ratios is far less than the polymerizations at lower ratios, as evidenced by slowly rising MWD and I^* values with an increase in the ratio. The I^* values of over 100% (145−193%, runs 18−20) are indicative of significant chain-transfer reactions at high $[MMA]_0/[4]_0$ ratios, but the catalyst is not deactivated as the polymerization can still proceed to high to near quantitative monomer conversions in longer times (4−5 h). Worth noting here is that the syndiotacticity of the resulting PMMA remained rather constant (88−90% rr) upon 10-fold variations of the monomer-to-catalyst ratio.

Kinetic experiments that employed the $[MMA]_0/[4]_0$ ratios ranging from 100 to 1000 (i.e., 10-fold variation in catalyst concentration) clearly show the first-order dependence on [MMA] for all the ratios (Figure 3). Furthermore, a double logarithm plot (Figure 4) of the apparent rate constants (k_{app}), obtained from the slopes of the best-fit lines to the plots of $\ln([MMA]_0/[MMA]_t)$ versus time as a function of $\ln[cat]_0$, was fit to a straight line ($R^2 = 0.96$) with a slope of 1.07. Thus, the kinetic order with respect to [cat], given by the slope of 1, reveals that the propagation is also first order in catalyst concentration, indicating that the MMA polymerization follows the monometallic, intramolecular coordination−addition mechanism, similar

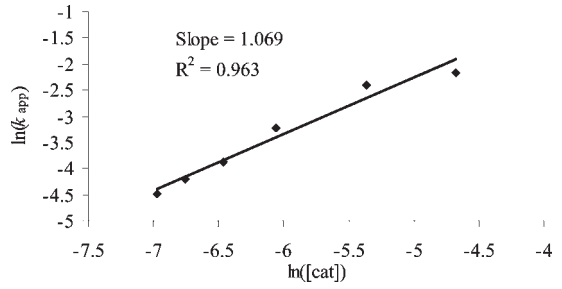

Figure 4. Plot of $\ln(k_{app})$ versus ln[catalyst] for the MMA polymerization by **4** in CH_2Cl_2 at 25 °C.

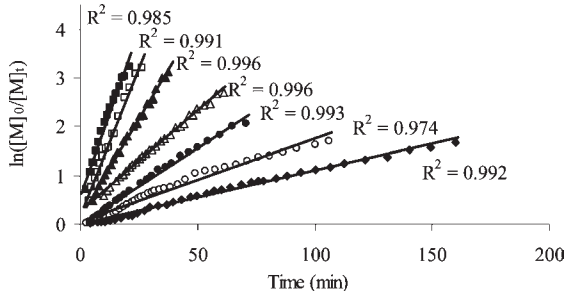

Figure 5. Plots of the first-order kinetics of $\ln([MMA]_0/[MMA]_t)$ versus time (min) for the polymerization of MMA by **4** in CD_2Cl_2 at different temperatures: 30 (■), 20 (□), 10 (▲), 0 (△), −10 (●), −20 (○), and −30 (◆) °C).

to that undergone by *ansa*-C_2-ligated[5c,5d] and C_s-ligated[14] catalysts we previously described in detail.

Polymerization Thermodynamic Parameters. To acquire activation enthalpy ($\Delta H^{\ddagger}$), entropy ($\Delta S^{\ddagger}$, and free energy ($\Delta G^{\ddagger}$), for the MMA polymerization reaction catalyzed by metallacycle **4**, we examined the polymerization reaction in CD_2Cl_2 with a fixed $[MMA]_0$:$[\mathbf{4}]_0$ ratio of 100:1 at varied temperatures from −30 to 30 °C. Using the transition-state theory expression for the rate constant: $k = (k_BT/h)\exp(-\Delta H^{\ddagger}/RT)\exp(\Delta S^{\ddagger}/R)$, we obtained the apparent rate constant for each temperature run from first-order kinetic plots of $\ln([MMA]_0/[MMA]_t)$ versus time at that given temperature (Figure 5). A plot of $\ln(hk/k_BT)$ versus $1/T$ gave a straight line (R^2 = 0.98, Figure 6), the slope and intercept of which yielded $\Delta H^{\ddagger}$ (= $-R \times$ slope) = 6.23 kcal/mol and $\Delta S^{\ddagger}$ (= $R \times$ intercept) = −41.7 eu, respectively. Hence, the enthalpic activation barrier for the polymerization reaction is quite low (6.23 kcal/mol), but due to a large negative entropic contribution (which is consistent with the associative displacement of the coordinated penultimate ester group by incoming monomer, i.e., ring-opening of the chelate, being the rate-determining step in the propagation "catalysis" cycle[10]), the calculated activation free energy $\Delta G^{\ddagger}$ is much larger (17.6 kcal/mol at 273 K).

We further examined the effects of polymerization temperature on syndiospecificity of the MMA polymerization by catalyst **4** in both CH_2Cl_2 and toluene (Table 3). For the polymerization in CH_2Cl_2, raising the polymerization temperature from 25 to 50 °C lowered the syndiotacticity by ~3% to 87% rr (run 21 vs 22, Table 3). On the other hand, lowering the polymerization temperature from 25 to 0 °C increased the syndiotacticity by ~4% to 94% rr (run 23 vs 22, Table 3) at the expense of reactivity and initiator efficiency reduction. Intriguingly, the polymerization in toluene revealed an opposite trend: raising the polymerization

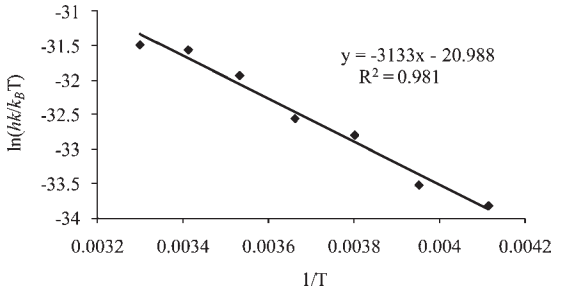

Figure 6. Plot of $\ln(hk/k_BT)$ versus $1/T$ for the polymerization of MMA by **4** in CD_2Cl_2.

temperature from 25 to 50 °C actually enhanced the syndiotacticity by ~4% to 91.6% rr (91.8% rr for a repeat; run 24 vs 25, Table 3).

Effects of the Activator $B(C_6F_5)_3$ on Chain Transfer. As $[HB(C_6F_5)_3]^-$-based catalysts can trigger chain-transfer reactions (vide supra), we further examined the potential effects of the activator $B(C_6F_5)_3$ to the precatalyst **4** ratio, the results of which were summarized in Table 4. For polymerizations carried out in CH_2Cl_2, chain transfer was not noticeable with a 1:1 $[B(C_6F_5)_3]$/[pre-**4**] ratio (97.8% I^*, run 26). Intriguingly, an increase of the ratio to 2:1 brought about significant chain transfer to this polymerization system (417% I^*) and also significantly lowered the polymer syndiotacticity (82.4% rr), which was accompanied by the increased molecular weight distribution (2.49 MWD), run 27. A further increase in the ratio to 5 did not result in additional significant changes in either chain transfer or syndiotacticity (run 28 vs 27).

A similar trend was also observed for the polymerizations carried out in toluene (runs 29−31), but chain transfer was much more pronounced (approximately by a factor of 2). Specifically, an increase of the $[B(C_6F_5)_3]$/[pre-**4**] ratio from 1:1 (218% I^*, 87.5% rr, run 29) to 2:1 (695% I^*, 76.6% rr, run 30) drastically increased chain transfer while concomitantly lowering the polymer syndiotacticity. Again, a further increase in the ratio from 1 to 5 showed much less additional impact on chain transfer and a minor effect on syndiotacticity (run 31 vs 30). Comparative polymerizations using the preactivation and the in-reactor activation methodology (see Experimental Section) gave rather similar results. Significantly, the quenched/purified polymer sample derived from substantial chain-transfer reactions (the run with 2 equiv of the borane) now exhibits peaks in ^{1}H NMR (Figure 7) at δ 6.18, 5.43 (CH_2=) and δ 3.68 (−OCH_3), which are rather similar to the MMA monomer peaks (except that the methyl group is now a polymer group) but clearly not from the monomer by our control experiments, for a vinylidene chain end, −C(CO-OMe)=CH_2. On the other hand, the PMMA samples derived from the polymerizations without noticeable chain transfer (e.g., run 26) contained no such unsaturated chain ends.

To further confirm the chain-end groups of the PMMA produced by the chain-transfer polymerization promoted by the anion $[HB(C_6F_5)_3]^-$, an isolated low MW sample produced by catalyst **4** in toluene with a $[B(C_6F_5)_3]$/[pre-**4**] ratio of 2 was characterized by MALDI-TOF mass spectrometry. The plot of m/z values of the peaks vs the number of MMA repeat units yielded a perfectly straight line, giving a slope of 100 and an intercept of 123 (Figure 8). The slope corresponds to the molar mass of the MMA monomer, whereas the intercept is the sum of the masses of Na^+ (from the added NaI) and end groups, which correspond to just an additional MMA unit. This analysis clearly shows that the polymer has a

Table 3. Selected MMA Polymerization Results by Catalyst 4[a]

run no.	solvent	temp (°C)	time (h)	conv. (%)	$10^{-3}M_n$ (g/mol)	MWD (M_w/M_n)	I^* (%)	[rr] (%)	[mr] (%)	[mm] (%)
21	CH_2Cl_2	50	1.5	87.8	32.8	1.32	108	87.3	10.5	2.2
22	CH_2Cl_2	25	1.5	97.2	40.1	1.39	97.8	90.5	7.7	1.8
23	CH_2Cl_2	0	5	49.2	44.6	1.29	44.7	94.1	4.5	1.4
24	toluene	50	1.5	57.4	38.5	1.36	59.7	91.6	6.5	1.9
25	toluene	25	24	95.4	17.7	1.63	218	87.5	10.6	1.9

[a] $[MMA]_0$ = 0.935 M and $[precatalyst]_0 = [B(C_6F_5)_3]_0$ = 2.34 mM for a [MMA]:[catalyst] ratio of 400:1; see footnotes in Table 1 for explanation of abbreviations.

Table 4. MMA Polymerization Results by Catalyst 4 with Varied $[B(C_6F_5)_3]/[pre\text{-}4]$ Ratios[a]

run no.	solvent	$[B(C_6F_5)_3]/[pre\text{-}4]$	time (h)	conv. (%)	$10^{-3}M_n$ (g/mol)	MWD (M_w/M_n)	I^* (%)	[rr] (%)	[mr] (%)	[mm] (%)
26	CH_2Cl_2	1	1.5	97.2	40.1	1.39	97.8	90.5	7.7	1.8
27	CH_2Cl_2	2	1.5	98.7	9.52	2.49	417	82.4	15.1	2.5
28	CH_2Cl_2	5	1.5	98.5	9.18	2.18	432	82.0	15.6	2.4
29	toluene	1	24	95.4	17.7	1.63	218	87.5	10.6	1.9
30	toluene	2	24	>99	5.79	2.07	695	76.6	20.7	2.7
31	toluene	5	24	>99	5.25	2.12	767	77.5	19.8	2.7

[a] $[MMA]_0$ = 0.935 M and $[pre\text{-}4]_0$ = 2.34 mM for a [MMA]:[Zr] ratio of 400:1; see footnotes in Table 1 for explanation of abbreviations.

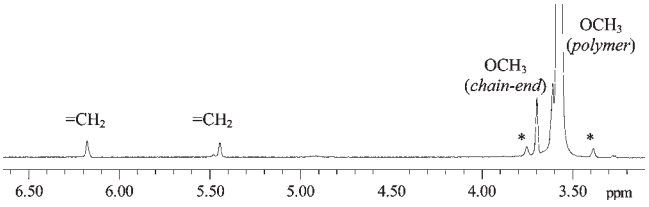

Figure 7. Portion of ^1H NMR spectrum ($CDCl_3$) of PMMA (run 30, Table 4). Peaks marked with "*" are spinning sidebands of the highly intense signal of the polymer OCH_3 group.

structural formula of $[H-(MMA)_n-CH_2C(COOMe)=CH_2]$, where the initiation chain end is H and the termination chain end is $-CH_2C(COOMe)=CH_2$ (Figure 8).

Computational Rationalization of Unique Polymerization Behavior of $[HB(C_6F_5)_3]^-$-Based Catalysts. In this section, we provide a computational rationalization of the experimental observations, especially concerning some unique effects of the anion $[HB(C_6F_5)_3]^-$ on the MMA polymerization activity and the resulting polymer stereoregularity as well as chain transfer, as compared to other more commonly used, weakly coordinating anions such as $[MeB(C_6F_5)_3]^-$ and $[B(C_6F_5)_4]^-$. With this goal in mind, we first compared the atomic charges on the free anions (Table 5), the ion pair (IP) dissociation energy, and the IP neutralization energy based on catalyst **1**. We also investigated alternative coordination geometries for $[HB(C_6F_5)_3]^-$ (Scheme 3) and how the structure of the catalyst influences the way the counterion approaches the metal (Scheme 4). Analysis of the Hirshfeld atomic charges[39] indicates that the H atom in $[HB(C_6F_5)_3]^-$, with a charge of −0.09e, is quite less charged than the Me group in $[MeB(C_6F_5)_3]^-$, with a total charge of −0.20e. Furthermore, as compared to the other two counterions, the B atom in $[HB(C_6F_5)_3]^-$ is somewhat negatively charged, which means that the C_6F_5 groups in $[HB(C_6F_5)_3]^-$ are not able to withdraw completely the excess charge from the B atom. Consequently, the charges on the F atoms are largely the same in all the counterions. On a geometrical ground, the B−H bond in free $[HB(C_6F_5)_3]^-$, 1.21 Å, is shorter than the B−Me bond in free $[MeB(C_6F_5)_3]^-$, 1.64 Å, which suggests that the anion $[HB(C_6F_5)_3]^-$ should approach the Zr center of the catalysts more than $[MeB(C_6F_5)_3]^-$ to engage properly in catalyst−counterion interaction, and thus steric clashes between a bulky ligand and the counterion could compromise the IP strength. In short, the reduced charge on the H atom and the short B−H bond in $[HB(C_6F_5)_3]^-$ suggest that this counterion could actually be less coordinating than the $[MeB(C_6F_5)_3]^-$ counterion with bulky catalysts.

Considering the behavior of systems **1** and **4** in the presence of an ester-enolate growing chain, again we compared $[HB(C_6F_5)_3]^-$ to $[MeB(C_6F_5)_3]^-$ and, when possible, to $[B(C_6F_5)_4]^-$. The data are summarized in Scheme 3. As a reference structure, we considered the counterion coordinated IP species **A**, at 0 kcal/mol. The first clear result is that the most stable species, whatever solvent or counterion is considered, are the eight-membered chelate species **B** and the MMA coordinated species **C**. As expected, these species are of comparable energy, although the MMA coordinated species is disfavored by entropic effects, which are not considered in the present calculations.

Moving to the strength of the IP, calculations clearly indicate a weaker coordination ability of $[HB(C_6F_5)_3]^-$ relative to $[MeB(C_6F_5)_3]^-$, demonstrated by the IP dissociation energy leading to **E** in Scheme 3. The gas-phase value for $[HB(C_6F_5)_3]^-$, for both **1** and **4**, is intermediate between those for $[MeB(C_6F_5)_3]^-$ and $[B(C_6F_5)_4]^-$. Of course, solvent polarity decreases the energy required to dissociate the ion pairs, but in any case $[HB(C_6F_5)_3]^-$ is calculated to be less coordinating than $[MeB(C_6F_5)_3]^-$. Interestingly, the stability of **B** and **C**, as well as the IP dissociation energy, is only slightly dependent on the catalyst bulkiness. This behavior can be ascribed to the preferential coordination of $[HB(C_6F_5)_3]^-$ through a F atom rather than the H atom (vide infra). Last, we also evaluated the neutralization energy, which is the energy required to abstract H or Me from the corresponding counterion to form the neutral species **D**. According to the values reported in Scheme 3, neutralization is not favored over the IP and is much more disfavored relative to species **B** and **C**. Overall, this analysis further shows that considering the possibilities illustrated in Scheme 3, catalysts paired with $[HB(C_6F_5)_3]^-$, at odd with the experimental results (from an anion coordinating aptitude point of view), should behave similarly to ones paired with $[B(C_6F_5)_4]^-$, or between $[MeB(C_6F_5)_3]^-$ and

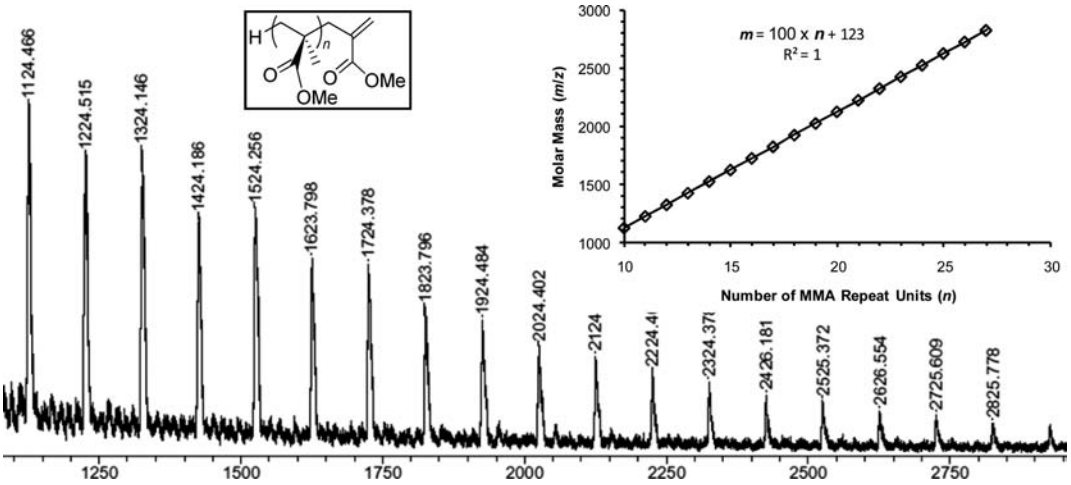

Figure 8. MALDI-TOF mass spectrum of the isolated low-MW PMMA produced by catalyst **4** in toluene with a $[B(C_6F_5)_3]$/[pre-**4**] ratio of 2. Inset, left: PMMA structure with chain-end groups. Inset, right: Plot of m/z values versus the number of MMA repeat units (n).

Table 5. Hirshfeld Atomic Charges of the $[HB(C_6F_5)_3]^-$, $[MeB(C_6F_5)_3]^-$, and $[B(C_6F_5)_4]^-$

	$[HB(C_6F_5)_3]^-$	$[MeB(C_6F_5)_3]^-$	$[B(C_6F_5)_4]^-$
B	−0.06	0.00	0.00
H or Me	−0.09	−0.20	
C-ipso	−0.08	−0.08	−0.09
C-ortho	0.06	0.06	0.06
C-meta	0.04	0.04	0.04
C-para	0.04	0.04	0.05
F-ortho	−0.08	−0.07	−0.07
F-meta	−0.10	−0.10	−0.09
F-para	−0.09	−0.09	−0.09

$[B(C_6F_5)_4]^-$. Therefore, the peculiar MMA polymerization behavior of the catalysts paired with $[HB(C_6F_5)_3]^-$ is not a consequence of a stronger catalyst−counterion interaction.

Next, we considered if $[HB(C_6F_5)_3]^-$ can approach the metal center with the F atoms, as in the metallocene alkyl cations paired with $[HB(C_6F_5)_3]^-$ and $[B(C_6F_5)_4]^-$,[40] rather than through the B−H bond. This point arises from considering that the B−H bond is significantly shorter than the B−Me bond and that the Zr···HB$(C_6F_5)_3^-$ coordination distance would be similarly shorter than the Zr···MeB$(C_6F_5)_3^-$ coordination distance. Because a shorter cation−counterion distance calls for increased steric repulsion, we compared systems **1** and **4**. These results, shown in Scheme 4, clearly indicate that the two possible coordination geometries of [HB$(C_6F_5)_3]^-$ are competitive for **1**, with the F-coordination geometry favored by only 0.8 kcal/mol (55.5 vs 56.3 kcal/mol). The similar energy of the two geometries originates from the reduced charge on the H atom in $[HB(C_6F_5)_3]^-$ relative to that on the Me group of MeB$(C_6F_5)_3^-$ and from the reduced Zr···HB$(C_6F_5)_3^-$ distance relative to the Zr···MeB$(C_6F_5)_3^-$, both effects of which decrease the stability of the B−H bond coordination geometry. Moving to **4** the bulkiness of the ^{t}Bu groups further prevents an ideal approach of the B−H bond to the metal for engaging in the Zr···H interaction; see the larger Zr···B distance (3.48 vs 3.59 Å) and the rather lower IP dissociation energy (41.8 vs 51.8 kcal/mol) in **4** relative to those in **1** shown in Scheme 4 (left column). As a consequence, in case of **4** coordination of $[HB(C_6F_5)_3]^-$ through one of the meta F atoms is preferred by 10 kcal/mol, and the counterion is more similar to $[B(C_6F_5)_4]^-$. On the other hand, the increased bulkiness of **4** presents no problem for $[MeB(C_6F_5)_3]^-$, because the counterion is roughly 1 Å farther away and the IP dissociation energy is slightly affected (62.5 vs 60.2 kcal/mol).

The above analysis clearly highlights remarkable differences between $[HB(C_6F_5)_3]^-$ and $[MeB(C_6F_5)_3]^-$ in the case of methacrylate polymerization. Although the eight-membered resting state is the most stable species, $[HB(C_6F_5)_3]^-$ can exist in a variety of forms of comparable stability, and this behavior also depends on the catalyst steric pressure, indicative of a potentially reactive and multifaceted behavior. In comparison, $[MeB(C_6F_5)_3]^-$ and $[B(C_6F_5)_4]^-$ are rather stable and innocent counterions. Therefore, the unique polymerization behavior of $[HB(C_6F_5)_3]^-$-based catalysts, especially their ability to effect chain transfer, must have to do with the hydride in the anion. We reasoned that after MMA coordination, rather than proceeding to the chain-growth step by Michael addition, hydride addition of $[HB(C_6F_5)_3]^-$ to the coordinated monomer could generate a neutral bis(enolate) complex (which is the reverse of the vinylogous hydride abstraction shown in Scheme 2). The formed dormant bis(enolate) can then be reactivated toward chain growth by vinylogous hydride abstraction (Scheme 5). Considering that the two enolate ligands are now different, one being the growing-chain enolate, the other being a MMA-enolate, the consequence of the reaction depends on which enolate undergoes hydride abstraction. If the hydride is abstracted from the just formed MMA-enolate species, this H-addition/abstraction sequence has no consequence on either M_n or I^*. However, more importantly, if the hydride is abstracted from the growing-chain enolate species and the formed oligomeric or polymeric PMMA with a terminal double bond is displaced by another MMA molecule, this hydride-addition/abstraction sequence through the boron center results in a net chain-transfer reaction. This proposed mechanism exhibits some resemblance to that proposed for the catalytic chain transfer in free-radical polymerization by cobalt catalysts, which promote hydrogen atom abstraction (from chain radicals) and addition (to monomer) sequence.[41] On the other hand, the novel features of the current mechanism are also apparent in that the anion $[HB(C_6F_5)_3]^-$ donates the hydride for its addition to the monomer coordinated to the metal center and subsequently the resulting borane abstracts the hydride back from the enolate ligand on the metal (Scheme 5).

Scheme 3. Energetics (kcal/mol) Involved in Possible Transformations of the IP in Catalyst Systems 1 and 4[a]

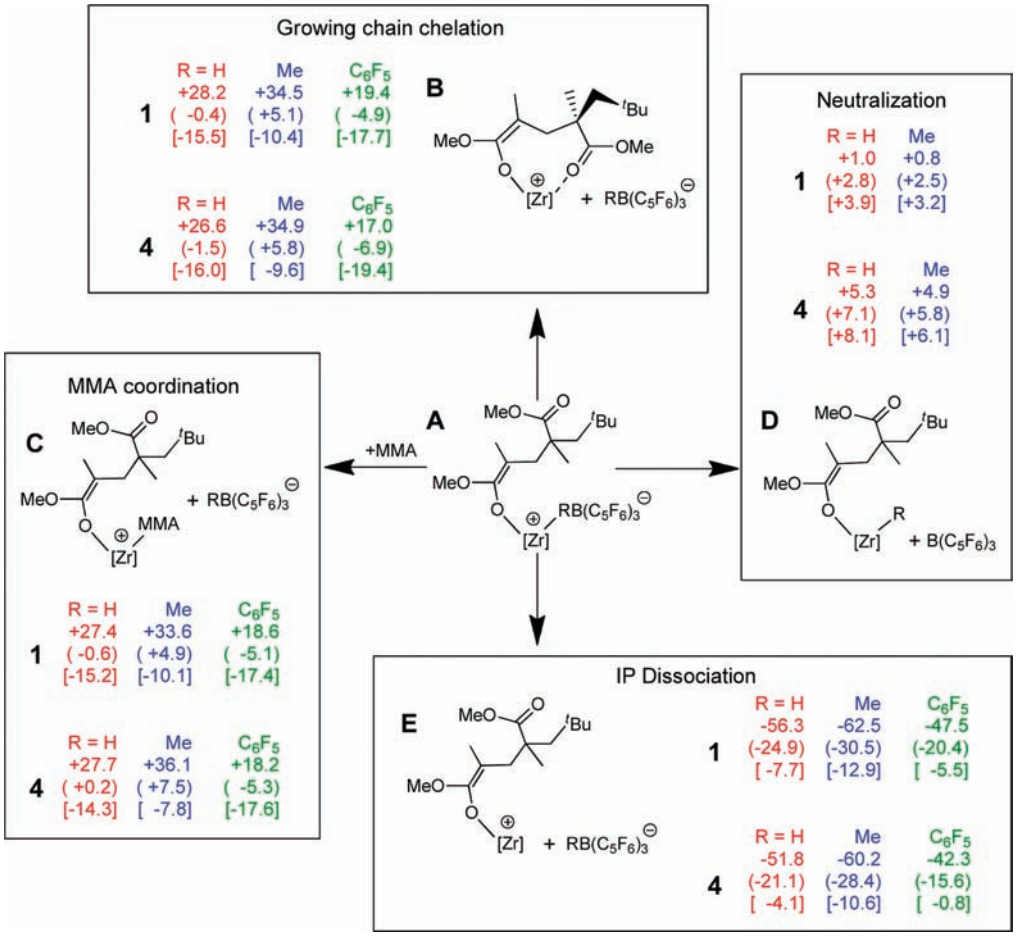

[a] Values are reported without parentheses for gas phase, in round parentheses (toluene), and in square brackets [CH_2Cl_2].

Scheme 4. Zr···B and Zr···F Distances (Å) and IP Dissociation Energy (kcal/mol) in the Gas Phase for Alternative IP Coordination Geometries for $[HB(C_6F_5)_3]^-$ and $[MeB(C_6F_5)_3]^-$

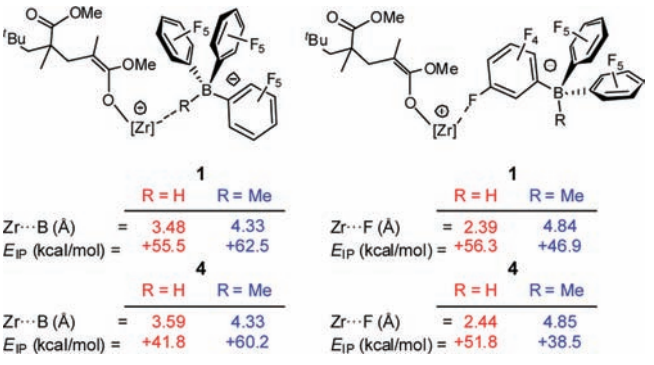

To examine the feasibility of this mechanism, we calculated the energy of all the species described in Scheme 5. As anticipated, the MMA coordinated species **G** is nearly isoenergetic with the eight-membered chelate resting state **F**, and solvent polarity has a negligible effect on this step. A Michael addition chain growth reaction, leading to **H**, normally is the fate of the MMA coordination intermediate **G**.[14,30] However, $[HB(C_6F_5)_3]^-$ can uniquely donate the hydride to the coordinated MMA molecule, leading to the neutral bis(enolate) species **I**, which is clearly favored in the gas phase because of the formation of neutral species. Solvent effects have thus a clear impact on the thermodynamics of this step. In fact, in toluene, **I** becomes slightly favored over **G**, whereas in CH_2Cl_2 **G** is slightly favored. The dormant state, bis(enolate) species **I**, can be reactivated by hydride-abstraction with the borane released from the prior hydride addition step. If the hydride is abstracted from the MMA-enolate, the H-addition/abstraction is nonproductive. However, if the hydride is abstracted from the growing chain-enolate, **I** is converted into **J**, and the vinyl-terminated PMMA chain can be displaced by another MMA molecule, leading to **K**, from which Michael addition, leading to **L**, starts a new PMMA chain. Based on the energy values reported in Scheme 5, the key step of this H-shuttling chain-transfer pathway, **I** to **J**, is disfavored over hydride abstraction **I** to **G**, which is qualitatively consistent with the formation of high molecular weight PMMA under normal conditions. Significantly, the strong dependence of the energetics in Scheme 5 on solvent polarity is in qualitative agreement with the experiments, which showed a considerably higher amount of chain transfer observed in toluene. Furthermore, the observed much more pronounced chain transfer in both toluene and CH_2Cl_2 in the presence of excess of the borane activator (vide supra) can be explained by this mechanism by virtue of shifting the equilibrium

Scheme 5. Energetics (kcal/mol) of Hydride-Shuttling Chain-Transfer Reaction for 1[a]

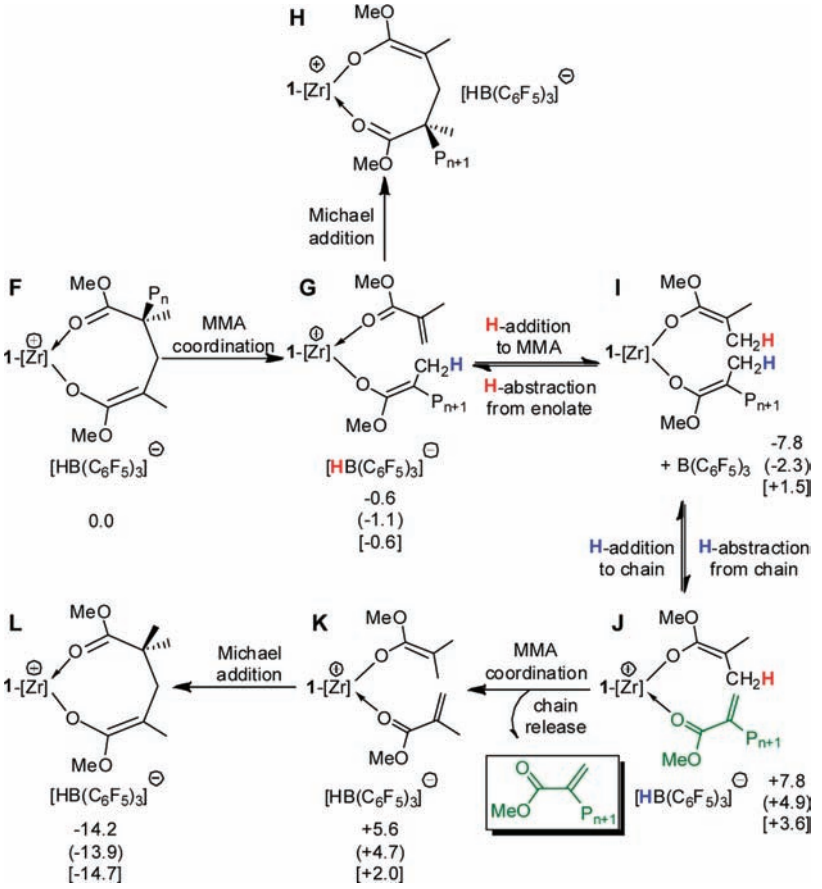

[a] Values are reported without parentheses for gas phase, in round parentheses (toluene), and in square brackets [CH_2Cl_2].

toward **J**. The observation that catalysts under conditions promoting more significant chain-transfer reactions produce polymers with lower syndiotacticity can be related to the more pronounced chain epimerization events.[12,14] Last, this H-shuttling mechanism also explains the formation of the experimentally observed PMMA chain terminated with an olefinic end group.

CONCLUSIONS

In summary, this contribution presented the ambient-temperature, quantitative-yield synthesis of 12 cationic group IV metallocene ester enolate eight-membered metallacycles from activation of their respective bis(ester enolate) precursors with $B(C_6F_5)_3$. The importance of such cationic chelates is apparent because their structures serve as suitable models for the active propagating species (resting state) involved in the methacrylate polymerization catalyzed by cationic metallocene catalysts. Additionally, clean generation of the such stable chelating cations paired with the anion $[HB(C_6F_5)_3]^-$ allowed us to uncover several unique MMA polymerization features of the cationic catalysts associated with this anion, which has not been recognized before this study. Most significantly, the current catalyst system led to the discovery of a novel chain-transfer pathway, the hydride-shuttling chain-transfer mechanism effected by the hydridoborate anion involving a hydride addition and abstraction sequence through the borane center.

This highly efficient synthesis of such cationic metallacycles is enabled by a rapid two-step reaction consisting of vinylogous hydride abstraction from the methyl group of the enolate $[OC(O^iPr)=CMe_2]$ moiety by $B(C_6F_5)_3$ to form the anion $[HB(C_6F_5)_3]^-$ and the resulting isopropyl methacrylate coordinated to metal, followed by subsequent nucleophilic addition of the second enolate ligand on metal to this coordinated isopropyl methacrylate. The scope of this activation methodology has been examined by extending group IV metallocene bis(ester enolate) substrates that varied metals (Ti, Zr, Hf), bridging atoms ($Ph_2C<$, $Ph_2Si<$, $Me_2C<$, $-CH_2CH_2-$), substituents (^{t}Bu, Et_3Si), substitution patterns (on 3-Cp and 2,7-Flu ring positions), and ligand symmetries (C_2, C_{2v}, C_1, and C_s), all of which led to the clean formation of their corresponding cationic metallacycles.

Comparative MMA polymerization studies by the above series of chelating cations paired with the same anion $[HB(C_6F_5)_3]^-$ under the same conditions revealed that the $Ph_2C<$ bridged, 2,7-di-*tert*-butyl-substituted Flu catalyst **4** is the most active, efficient, and syndiospecific catalyst. Kinetic experiments at room temperature show the MMA polymerization by **4** in CH_2Cl_2 follows first-order kinetics in both monomer and catalyst concentrations, consistent with a monometallic, intramolecular coordination−addition mechanism that involves in the propagation "catalysis" cycle the fast intramolecular Michael addition within the catalyst−monomer complex leading to the resting eight-membered ester enolate chelate, followed by the slower, rate-limiting ring-opening of the chelate to regenerate the active species. Polymerization reactions by metallacycle **4** performed at different temperatures have yielded activation enthalpy ($\Delta H^{\ddagger}$ = 6.23 kcal/mol), entropy ($\Delta S^{\ddagger}$ = −41.7 eu), and

free energy ($\Delta G^{\ddagger}$ = 17.6 kcal/mol at 273 K), showing a small enthalpic activation barrier, but a large negative entropic contribution, for the polymerization reaction.

In contrast to *ansa*-Flu-Cp ligated, eight-membered chelating cations paired with more commonly used, weakly coordinating anions such as $[MeB(C_6F_5)_3]^-$, $[B(C_6F_5)_4]^-$, and $[TRISPHAT]^-$, whose polymerization activity and syndiospecificity are insensitive to anion structure and solvent polarity, the same cations paired with the anion $[HB(C_6F_5)_3]^-$ show drastic activity differences in different solvents, with the activity in toluene being ~16-fold lower than that in CH_2Cl_2. In comparison, the $[HB(C_6F_5)_3]^-$-based catalysts also exhibit significantly lower activity (by 6−40-fold) and produce PMMA with noticeably lower syndiotacticity (by 4−7% rr). Most significantly, $[HB(C_6F_5)_3]^-$-based catalysts bring out substantial internal chain-transfer reactions, especially for the polymerizations carried out in toluene and in the presence of excess $B(C_6F_5)_3$, thereby releasing polymer chains with a terminal double bond and effecting a catalytic polymerization.

Computational results showed the thermodynamic feasibility of the activation steps, indicating that hydride abstraction is clearly favored over borane electrophilic attack to the C═C double bond of the enolate. Systematic comparisons of $[HB(C_6F_5)_3]^-$, $[MeB(C_6F_5)_3]^-$, and $[B(C_6F_5)_4]^-$ indicated that the coordination behavior of $[HB(C_6F_5)_3]^-$ should be intermediate between those of $[MeB(C_6F_5)_3]^-$ and $[B(C_6F_5)_4]^-$. On the other hand, calculations indicated that $[HB(C_6F_5)_3]^-$ can uniquely act as a weak hydride donor, thus promoting chain transfer.

AUTHOR INFORMATION

Corresponding Author
lcavallo@unisa.it; eugene.chen@colostate.edu

ACKNOWLEDGMENT

This work was supported by the National Science Foundation (NSF-1012326) for the work carried out at Colorado State University. L.Cav. thanks the HPC team of Enea (www.enea.it) for use of the ENEA-GRID and the HPC facilities CRESCO (www.cresco.enea.it) in Portici, Italy. We thank Boulder Scientific Co. for the research gifts of $B(C_6F_5)_3$, $[Ph_3C][B(C_6F_5)_4]$, and $[Ph_2C(Cp)(Flu)]ZrCl_2$.

REFERENCES

(1) Chen, E. Y.-X. *Chem. Rev.* **2009,** *109*, 5157–5214.

(2) Insertion oligomerization of acrylates: (a) Guironnet, D.; Caporaso, L.; Neuwald, B.; Göttker-Schnetmann, I.; Cavallo, L.; Mecking, S. *J. Am. Chem. Soc.* **2010,** *132*, 4418–4426. (b) Guironnet, D.; Roesle, P.; Rünzi, T.; Göttker-Schnetmann, I.; Mecking, S. *J. Am. Chem. Soc.* **2009,** *131*, 422–423.

(3) Selected reference works and reviews: (a) Chen, E. Y.-X.; Rodriguez-Delgado, A. In *Comprehensive Organometallic Chemistry III*; Bochmann, M., Vol. Ed.; Mingos, M. P., Crabtree, R. H., Chief Eds.; Elsevier: Oxford, 2007; Vol. 4, pp 759−1004. (b) Cuenca, T. In *Comprehensive Organometallic Chemistry III*; Bochmann, M., Vol. Ed.; Mingos, M. P., Crabtree, R. H., Chief Eds.; Elsevier: Oxford, 2007; Vol. 4, pp 323−696. (c) Bochmann, M. *J. Chem. Soc., Dalton Trans.* **1996,** 255–270. (d) Jordan, R. F. *Adv. Organomet. Chem.* **1991,** *32*, 325–387.

(4) Selected examples: (a) Zhang, Y.; Chen, E. Y.-X. *J. Organomet. Chem.* **2010,** *695*, 1464–1471. (b) Lian, B.; Thomas, C. M.; Navarro, C.; Carpentier, J.-F. *Organometallics* **2007,** *26*, 187–195. (c) Ning, Y.; Cooney, M. J.; Chen, E. Y.-X. *J. Organomet. Chem.* **2005,** *690*, 6263–6270. (d) Strauch, J. W.; Fauré, J.-L.; Bredeau, S.; Wang, C.; Kehr, G.; Fröhlich, R.; Luftmann, H.; Erker, G. *J. Am. Chem. Soc.* **2004,** *126*, 2089–2104. (e) Frauenrath, H.; Keul, H.; Höcker, H. *Macromolecules* **2001,** *34*, 14–19. (f) Karanikolopoulos, G.; Batis, C.; Pitsikalis, M.; Hadjichristidis, N. *Macromolecules* **2001,** *34*, 4697–4705. (g) Bandermann, F.; Ferenz, M.; Sustmann, R.; Sicking, W. *Macromol. Symp.* **2000,** *161*, 127–134. (h) Cameron, P. A.; Gibson, V.; Graham, A. J. *Macromolecules* **2000,** *33*, 4329–4335. (i) Deng, H.; Shiono, T.; Soga, K. *Macromolecules* **1995,** *28*, 3067–3073. (j) Collins, S.; Ward, S. G. *J. Am. Chem. Soc.* **1992,** *114*, 5460–5462.

(5) (a) Ning, Y.; Chen, E. Y.-X. *J. Am. Chem. Soc.* **2008,** *130*, 2463–2465. (b) Rodriguez-Delgado, A.; Mariott, W. R.; Chen, E. Y.-X. *J. Organomet. Chem.* **2006,** *691*, 3490–3497. (c) Rodriguez-Delgado, A.; Chen, E. Y.-X. *Macromolecules* **2005,** *38*, 2587–2594. (d) Rodriguez-Delgado, A.; Mariott, W. R.; Chen, E. Y.-X. *Macromolecules* **2004,** *37*, 3092–3100. (e) Bolig, A. D.; Chen, E. Y.-X. *J. Am. Chem. Soc.* **2004,** *126*, 4897–4906.

(6) (a) Stojcevic, G.; Kim, H.; Taylor, N. J.; Marder, T. B.; Collins, S. *Angew. Chem., Int. Ed.* **2004,** *43*, 5523–5526. (b) Nguyen, H.; Jarvis, A. P.; Lesley, M. J. G.; Kelly, W. M.; Reddy, S. S.; Taylor, N. J.; Collins, S. *Macromolecules* **2000,** *33*, 1508–1510. (c) Li, Y.; Ward, D. G.; Reddy, S. S.; Collins, S. *Macromolecules* **1997,** *30*, 1875–1883.

(7) (a) Lian, B.; Lehmann, C. W.; Navarro, C.; Carpentier, J.-F. *Organometallics* **2005,** *24*, 2466–2472. (b) Lian, B.; Toupet, L.; Carpentier, J.-F. *Chem.-Eur. J.* **2004,** *10*, 4301–4307.

(8) Lian, B.; Spanio, T. P.; Okuda, J. *Organometallics* **2007,** *26*, 6653–6660.

(9) (a) Miyake, G. M.; Caporaso, L.; Cavallo, L.; Chen, E. Y.-X. *Macromolecules* **2009,** *42*, 1462–1471. (b) Miyake, G. M.; Chen, E. Y.-X. *Macromolecules* **2008,** *41*, 3405–3416. (c) Miyake, G. M.; Mariott, W. R.; Chen, E. Y.-X. *J. Am. Chem. Soc.* **2007,** *129*, 6724–6725. (d) Mariott, W. R.; Chen, E. Y.-X. *Macromolecules* **2005,** *38*, 6822–6832. (e) Mariott, W. R.; Chen, E. Y.-X. *Macromolecules* **2004,** *37*, 4741–4743.

(10) Chen, E. Y.-X. *Dalton Trans.* **2009,** 8784–8793.

(11) Bandermann, F.; Ferenz, M.; Sustmann, R.; Sicking, W. *Macromol. Symp.* **2001,** *174*, 247–253.

(12) (a) Ning, Y.; Caporaso, L.; Correa, A.; Gustafson, L. O.; Cavallo, L.; Chen, E. Y.-X. *Macromolecules* **2008,** *41*, 6910–6919. (b) Ning, Y.; Zhu, H.; Chen, E. Y.-X. *J. Organomet. Chem.* **2007,** *692*, 4535–4544. (c) Ning, Y.; Chen, E. Y.-X. *Macromolecules* **2006,** *39*, 7204–7215.

(13) Chen, E. Y.-X. *Comments Inorg. Chem.* **2009,** *30*, 7–27.

(14) Zhang, Y.; Ning, Y.; Caporaso, L.; Cavallo, L.; Chen, E. Y.-X. *J. Am. Chem. Soc.* **2010,** *132*, 2695–2709.

(15) Spaether, W.; Klass, K.; Erker, G.; Zippel, F.; Fröhlich, R. *Chem.-Eur. J.* **1998,** *4*, 1411–1417.

(16) Zhang, Y.; Chen, E. Y.-X. *Macromolecules* **2008,** *41*, 36–42.

(17) Mariott, W. R.; Rodriguez-Delgado, A.; Chen, E. Y.-X. *Macromolecules* **2006,** *39*, 1318–1327.

(18) Allen, R. D.; Long, T. E.; McGrath, J. E. *Polym. Bull.* **1986,** *15*, 127–134.

(19) Feng, S.; Roof, G. R.; Chen, E. Y.-X. *Organometallics* **2002,** *21*, 832–839.

(20) (a) Lee, C. H.; Lee, S. J.; Park, J. W.; Kim, K. H.; Lee, B. Y.; Oh, J. S. *J. Mol. Catal. A: Chem.* **1998,** *132*, 231–239. (b) Biagini, P.; Lugli, G.; Abis, L.; Andreussi, P. U.S. Patent 5,602269, 1997.

(21) Rodriguez-Delgado, A.; Chen, E. Y.-X. *J. Am. Chem. Soc.* **2005,** *127*, 961–974.

(22) Jutzi, P.; Müller, C.; Stammler, A.; Stammler, H. *Organometallics* **2000,** *19*, 1442–1444.

(23) Kajigaeshi, S.; Kadowaki, T.; Nishida, A.; Fujisaki, S.; Noguchi, M. *Synthesis* **1984,** *4*, 335–337.

(24) Hopf, A.; Kaminsky, W. *Catal. Commun.* **2002,** *3*, 459–464.

(25) Rix, F. C. U.S. Patent 6, 506, 857 B2, 2003.

(26) Miller, S. A.; Bercaw, J. E. *Organometallisc* **2006,** *25*, 3576–3592.

(27) Patsidis, K.; Alt, H.; Milius, W.; Palackal, S. J. *J. Organomet. Chem.* **1996,** *509*, 63–71.

(28) Ewen, J. A.; Jones, R. L.; Razavi, A.; Ferrara, J. D. *J. Am. Chem. Soc.* **1988,** *110*, 6255–6256.

(29) (a) Brar, A. S.; Singh, G.; Shankar, R. *J. Mol. Struct.* **2004,** *703*, 69–81. (b) Bovey, F. A.; Mirau, P. A. *NMR of Polymers*; Academic Press: San Diego, CA, 1996. (c) Kawamura, T.; Toshima, N.; Matsuzaki, K. *Makromol. Chem., Rapid Commun.* **1993,** *14*, 719–724. (d) Chujo, R.; Hatada, K.; Kitamaru, R.; Kitayama, T.; Sato, H.; Tanaka, Y. *Polym. J.* **1987,** *19*, 413–424. (e) Ferguson, R. C.; Ovenall, D. W. *Macromolecules* **1987,** *20*, 1245–1248. (f) Ferguson, R. C.; Ovenall, D. W. *Polym. Prepr.* **1985,** *26*, 182–183. (g) Subramanian, R.; Allen, R. D.; McGrath, J. E.; Ward, T. C. *Polym. Prepr.* **1985,** *26*, 238–240.

(30) (a) Caporaso, L.; Cavallo, L. *Macromolecules* **2008,** *41*, 3439–3445. (b) Caporaso, L.; Gracia-Budra, J.; Cavallo, L. *J. Am. Chem. Soc.* **2006,** *128*, 16649–16654.

(31) (a) *ADF2007 User's Manual*; Theoretical Chemistry, Vrije Universiteit: Amsterdam, 2007. (b) Baerends, E. J.; Ellis, D. E.; Ros, P. *Chem. Phys.* **1973,** *2*, 41–51.

(32) Vosko, S. H.; Wilk, L.; Nusair, M. *Can. J. Phys.* **1980,** *58*, 1200–1211.

(33) Becke, A. D. *Phys. Rev. A* **1988,** *38*, 3098–3100.

(34) (a) Perdew, J. P. *Phys. Rev. B* **1986,** *33*, 8822–8824. (b) Perdew, J. P. *Phys. Rev. B* **1986,** *34*, 7406–7406.

(35) (a) Klamt, A.; Schüürmann, G. *J. Chem. Soc., Perkin Trans.* **1993,** 799–805. (b) Pye, C. C.; Ziegler, T. *Theor. Chem. Acc.* **1999,** *101*, 396–408.

(36) Garner, L. E.; Zhu, H.; Hlavinka, M. L.; Hagadorn, J. R.; Chen, E. Y.-X. *J. Am. Chem. Soc.* **2006,** *128*, 14822–14823.

(37) Yang, X.; Stern, C. L.; Marks, T. J. *Angew. Chem., Int. Ed. Engl.* **1992,** *31*, 1375–1377.

(38) Horton, A. D.; de With, J.; van der Linder, A. J.; van de Weg, H. *Organometallics* **1996,** *15*, 2672–2674.

(39) Hirshfeld, F. L. *Theor. Chem. Acc.* **1977,** *44*, 129–138.

(40) Chen, E. Y.-X.; Mark, T. J. *Chem. Rev.* **2000,** *100*, 1391–1434.

(41) Gridnev, A. A.; Ittel, S. D. *Chem. Rev.* **2001,** *101*, 3611–3659.